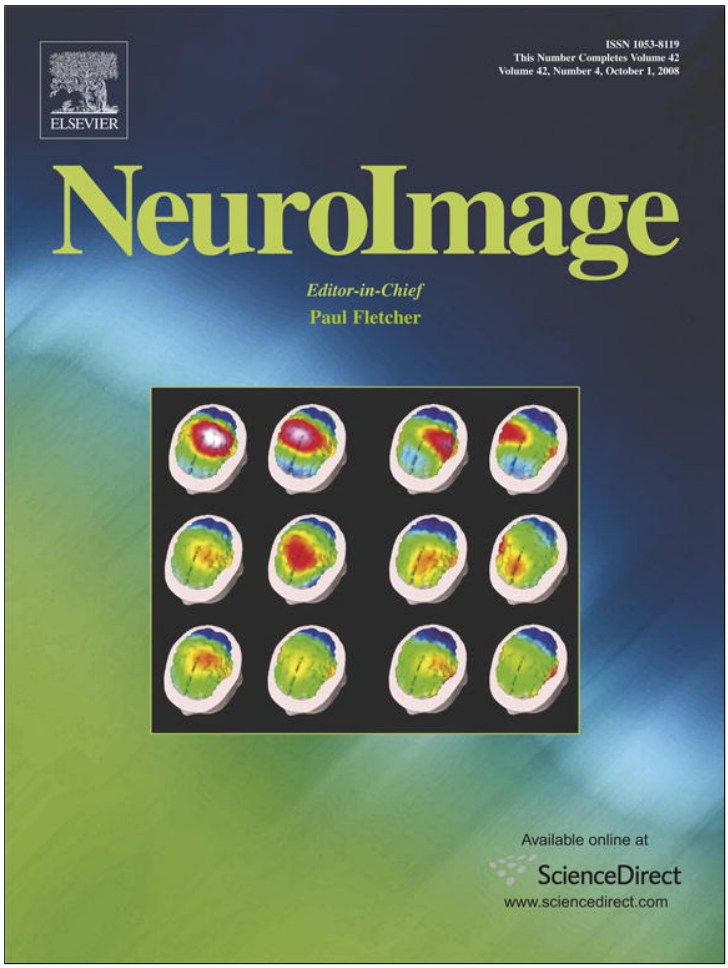

NeuroImage 42 (2008) 1397–1413

Contents lists available at ScienceDirect

NeuroImage

journal homepage: www.elsevier.com/locate/ynimg

Evaluation of hierarchical Bayesian method through retinotopic brain activities reconstruction from fMRI and MEG signals

Taku Yoshioka [a,b,*], Keisuke Toyama [b], Mitsuo Kawato [b], Okito Yamashita [b], Shigeaki Nishina [c], Noriko Yamagishi [a,b], Masa-aki Sato [b]

[a] National Institute of Information and Communications Technology, Japan
[b] ATR Computational Neuroscience Laboratories, Seika, Soraku, Kyoto 619-0288, Japan
[c] Boston University, 64 Cummington, Boston, MA 02215, USA

ARTICLE INFO

Article history:
Received 10 January 2008
Revised 6 June 2008
Accepted 9 June 2008
Available online 21 June 2008

ABSTRACT

A hierarchical Bayesian method estimated current sources from MEG data, incorporating an fMRI constraint as a hierarchical prior whose strength is controlled by hyperparameters. A previous study [Sato, M., Yoshioka, T., Kajihara, S., Toyama, K., Goda, N., Doya, K., Kawato, M., 2004. Hierarchical Bayesian estimation for MEG inverse problem. Neuroimage 23, 806–826] demonstrated that fMRI information improves the localization accuracy for simulated data. The goal of the present study is to confirm the usefulness of the hierarchical Bayesian method by the real MEG and fMRI experiments using visual stimuli with a fan-shaped checkerboard pattern presented in four visual quadrants. The proper range of hyperparameters was systematically analyzed using goodness of estimate measures for the estimated currents. The robustness with respect to false-positive activities in the fMRI information was also evaluated by using noisy priors constructed by adding artificial noises to real fMRI signals. It was shown that with appropriate hyperparameter values, the retinotopic organization and temporal dynamics in the early visual area were reconstructed, which were in a close correspondence with the known brain imaging and electrophysiology of the humans and monkeys. The false-positive effects of the noisy priors were suppressed by using appropriate hyperparameter values. The hierarchical Bayesian method also was capable of reconstructing retinotopic sequential activation in V1 with fine spatiotemporal resolution, from MEG data elicited by sequential stimulation of the four visual quadrants with the fan-shaped checker board pattern at much shorter intervals (150 and 400 ms) than the temporal resolution of fMRI. These results indicate the potential capability for the hierarchical Bayesian method combining MEG with fMRI to improve the spatiotemporal resolution of noninvasive brain activity measurement.

Introduction

Magnetoencephalography (MEG) directly measures the magnetic fields caused by neural current activity, with a high temporal resolution. Its spatial resolution, however, is poor because of the ill-posed nature of the inverse problem of estimating source currents from magnetic fields (Nunez, 1981). Therefore, prior information on source currents is essential in solving the inverse problem. Different types of methods have been proposed for reconstructing source currents with prior information.

On the basis of the observation that the principal source of MEG signals is postsynaptic current flow in pyramidal cells, the source currents creating MEG signals are often modeled as current dipoles (Hamalainen et al., 1993). Inverse procedures for estimating source currents from MEG signal are classified by how the current dipoles are defined. Equivalent current dipole (ECD) methods approximate the source currents by a small number of current dipoles (Aine et al., 2000; Hari, 1991; Miltner et al., 1994; Mosher et al., 1992; Scherg et al., 1999). The positions and orientations of the current dipoles are estimated with the current amplitudes from the MEG signals. Because of the assumption of a restricted number of current dipoles, ECD methods do not provide a fine spatiotemporal pattern of neural current activity.

On the other hand, distributed source methods assume a large number of current dipoles with fixed positions and orientations. Once the positions and orientations are fixed, the current amplitudes of the dipoles and the induced magnetic fields have a linear relationship. This is referred to as the forward model. On the basis of the linear relationship of the forward model, distributed source methods estimate the

* Corresponding author. National Institute of Information and Communications Technology, 2-2-2 Hikaridai, Seika, Soraku, Kyoto 619-0288, Japan. Fax: +81 774 95 1259.
E-mail address: taku-y@atr.jp (T. Yoshioka).

1053-8119/$ – see front matter © 2008 Elsevier Inc. All rights reserved.
doi:10.1016/j.neuroimage.2008.06.013

current amplitudes of the dipoles. Since the number of current dipoles in a distributed source method is often much larger than the number of MEG sensors, estimation of the dipole currents is an ill-posed problem. A number of methods such as the minimum norm method (Hamalainen and Ilmoniemi, 1994; Wang et al., 1992), the maximum smoothness method (Pascual-Marqui, 1999; Pascual-Marqui et al., 1994) and the minimum L1-norm method (Uutela et al., 1999) have been introduced to solve the ill-posed inverse problem. In addition, MRI and fMRI measurements have been used to provide anatomical and functional constraints (Dale et al., 2000; Dale and Sereno, 1993; Kajihara et al., 2004; Liu et al., 1998; Phillips et al., 2002; Schmidt et al., 1999). The anatomical constraint (MRI) provides information on the positions and orientations of the current dipoles according to the cytoarchitectonic knowledge that the cortical pyramidal cells are arranged in the gray matter perpendicular to the cortical surface (Dale and Sereno, 1993). The functional constraint (fMRI) gives information on the relative amplitudes of the dipole currents (Dale et al., 2000; Kajihara et al., 2004; Liu et al., 1998).

We previously proposed a hierarchical Bayesian framework for the distributed source method, in which fMRI information is introduced as a hierarchical prior of the variance for each dipole current (Sato et al., 2004). Since the prior current variances are estimated from MEG and fMRI data, our method is theoretically tolerant with respect to false-positive signals contained in the fMRI data. Our simulation study confirmed that the hierarchical Bayesian method gives much more precise estimation than the conventional methods, and that it is, in fact, tolerant with respect to false-positive prior information in fMRI signals.

In the hierarchical Bayesian method, the strength of the fMRI constraint can be controlled by the hyperparameters of the hierarchical prior. In the previous study, we used a non-informative prior, in which the fMRI information is incorporated only as the initial values of the prior current variances. We consider such a weak fMRI constraint to give a good estimation when all of the assumptions in hierarchical Bayesian estimation are correct and an accurate forward model is obtained. In the previous study, we actually used the same forward model for calculating the artificial MEG data and for estimating the dipole currents from those data.

The hierarchical Bayesian method is based on a number of assumptions: spatial sparseness and smoothness of the dipole currents, Gaussian observation noise, accurate cortical surface model from MRI, accurate coregistration between MEG and MRI coordinates, and so on. Since these assumptions may be violated in real data, using fMRI data for constraints would give better estimation accuracy. MEG and fMRI measurements, however, can be contradictory because of the intrinsic difference in measurement principles (Bandettini, 2000; Belliveau et al., 1991; Logothetis et al., 2001; Ogawa et al., 1990). In addition, it is practically impossible to conduct MEG and fMRI measurements under exactly the same conditions, including the experimental design and the apparatuses for the experiments. Therefore, the strength of the functional constraint must be appropriately controlled by tuning the hyperparameters. The proper range of the hyperparameters must be limited for practical application of the proposed method.

In the current study, we tested how well the hierarchical Bayesian method can estimate neural activities and evaluated the effect of the hyperparameters on estimation results with real data. To do this, we conducted MEG and fMRI experiments with visual stimuli presented in four visual quadrants. Although the true spatiotemporal pattern of the cortical activity is unknown, the functional localization and temporal patterns of neural activities have been well studied by fMRI (Dougherty et al., 2003; Tootell et al., 1997; Sereno et al., 1995). The temporal patterns of neural activities have also been investigated by ECD methods with the help of fMRI information (Ahlfors et al., 1999; Di Russo et al., 2001, 2005; Vanni et al., 2001, 2004). On the other hand, the estimation of the neural activities of early visual areas, with fine spatiotemporal resolution, is considered difficult for distributed source methods with anatomical constraints, because of the complex anatomical structure of the early visual areas. Therefore, our visual experiment provides a good testbed for evaluating our method.

To evaluate the proper range of hyperparameters, we introduced goodness measures for the spatial and temporal patterns of the estimated currents. The robustness with respect to false-positive activities in the fMRI information was also evaluated by introducing noisy priors, which were constructed from correct priors (i.e., real fMRI data) by adding artificial false-positive activities. We found the proper ranges of hyperparameters for correct and noisy priors. Our estimation results with appropriate hyperparameter values, which were in the proper range, showed the retinotopic organization and temporal dynamics in the early visual areas, consistent with previously reported physiological findings.

We further applied our method to MEG data elicited by a pseudo-rotatory visual stimulus, in which four quadrantal visual stimuli were sequentially presented with a stimulus onset asynchrony (SOA) of 400 or 150 ms, either of which is much shorter than the temporal resolution of fMRI. The estimation results showed retinotopic sequential activation in V1 with fine spatiotemporal resolution.

Materials and methods

Experiments were conducted on four healthy subjects (ages 23–30, three males and one female). All subjects gave written informed consent for the experimental procedures, approved by the ATR Human Subject Review Committee. All subjects had normal or corrected-to-normal visual acuity and normal visual fields and color vision.

Visual stimuli and apparatuses

In both the fMRI and MEG experiments, the visual stimuli had the same characteristics, in terms of shape, color, luminance and subtended angle, but the temporal sequences for stimulus presentation were optimized for each technique. The stimuli were presented in four visual quadrants: upper right (UR), lower right (LR), lower left (LL), and upper left (UL). The stimuli consisted of a physically isoluminant red and green checkerboard pattern (subtended angle, 7°; CIE coordinates, [0.346, 0.299] for red and [0.268, 0.336] for green; luminance, 26 cd/m^2) on a gray background with the same luminance (subtended angle, 10°×8°; CIE coordinate, [0.186, 0.455]; Fig. 1a). Gaps (subtended angle 1°) were inserted to facilitate separability of the cortical activities around the calcarine sulcus. A small circle was displayed on the center of the background (subtended angle, 0.1°) as a fixation point. The visual stimuli were generated using a PC and VSG2/5 (Cambridge Research Systems, UK).

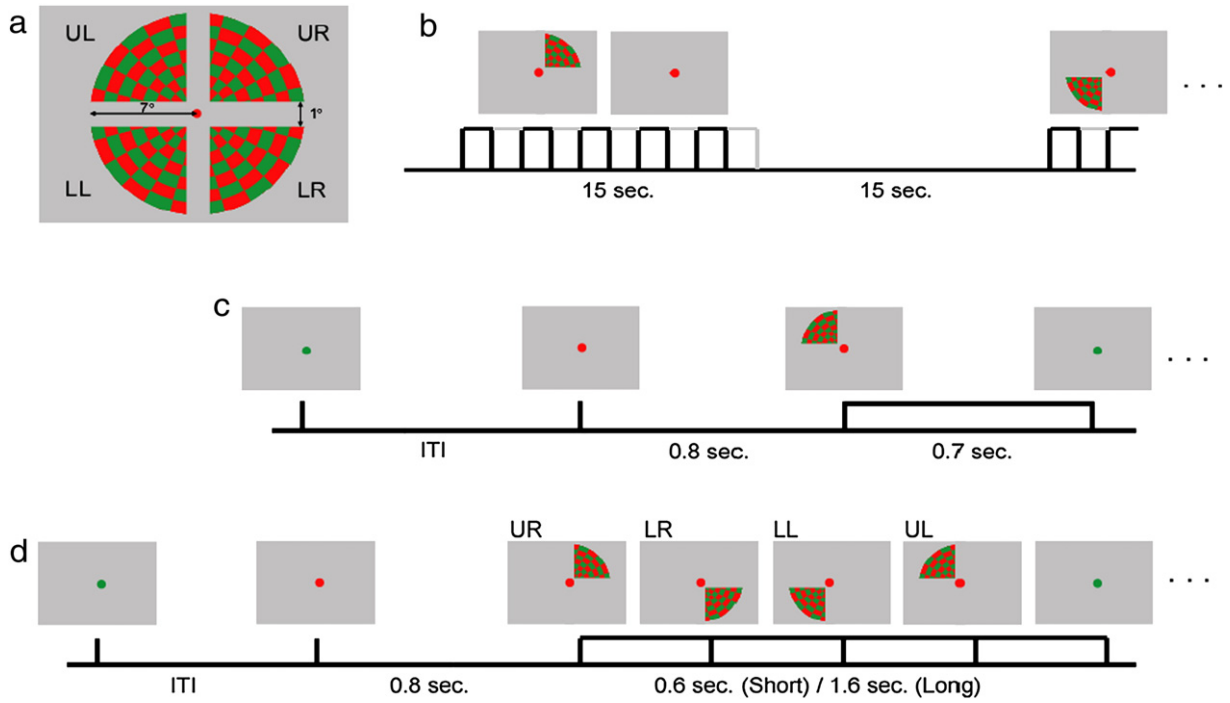

Fig. 1. Visual stimuli and task sequences in the fMRI and MEG experiments. (a) A fan-shaped stimulus was displayed in one of four visual quadrants (upper right (UR), lower right (LR), lower left (LL), and upper left (UL)). Each stimulus consisted of a red and green checkerboard pattern and had the same luminance as the background. (b) The block design employed in the fMRI experiment. In a block of 15 s, a pseudo-randomly selected stimulus was flashed five times at 1/3 Hz. The inter-block interval was also 15 s. (c) The randomized (RD) sequence in the MEG experiment, where a pseudo-randomly selected stimulus was displayed for 700 ms in a trial. The inter-trial interval varied randomly trial by trial between 1.5 and 2.5 s. (d) The pseudo-rotatory (RT) sequence in the MEG experiment. The UR, LR, LL, and UL quadrantal visual stimuli were sequentially presented for 400 ms or 150 ms (slow or fast condition, respectively).

In the fMRI experiments, the visual stimuli were back-projected onto a screen from outside a magnetically shielded room, by using an LCD projector (DLA-G150CL, Victor Company of Japan) and mirrors. The subjects viewed the projected images through a mirror attached to the head coil of the MRI scanner (viewing distance, 39 cm). In the MEG experiments, the visual stimuli were back-projected onto a screen from outside the magnetically shielded room through a glass window, by using an LCD projector (ELP-710, Epson, Japan). In this case, the subjects directly saw the screen (viewing distance, 170 cm). Although the viewing distance differed in the MEG and fMRI experiments, the subtended visual angles for the corresponding visual patterns were kept the same by adjusting the physical projection size.

Task design

The fMRI experiments were conducted with a block design (Fig. 1b). In each block, a fan-shaped stimulus (Fig. 1a) was presented in a quadrant five times at 3-s intervals (1.5 s with the stimulus followed by 1.5 s without the stimulus). The quadrants were pseudo-randomly selected and counter-balanced across blocks. The inter-block interval was 15 s. One session consisted of 12 blocks. For each subject, four sessions were conducted, and the total experimental time was nearly 24 min.

In the MEG experiments, we employed randomized (RD) and pseudo-rotatory (RT) sequences. In the RD sequence, a fan-shaped stimulus was presented in a pseudo-randomly selected quadrant for each trial (Fig. 1c). The subjects were asked not to blink their eyes during a trial. The fixation point's color changed from green to red 800 ms before the stimulus onset, which allowed the subject to know the start of each trial. The duration of the stimulus presentation was 700 ms. Magnetoencephalograms were recorded before (−300 to 0 ms) and after (0 to 700 ms) the stimulus onset. The inter-trial interval was pseudo-randomly varied between 1.5 and 2.5 s. One session consisted of 100 trials, and four sessions were conducted for each subject. The total time of the experiment with the RD sequence was about 25 min, including 1-min rest periods between sessions.

In the RT sequence, the fan-shaped patterns were presented sequentially clockwise in each of the quadrants with a stimulus onset asynchrony (SOA) of 400 ms (slow) or 150 ms (fast) (Fig. 1d). The SOA was fixed within each session. The time schedule before the stimulus presentation in the RT sequence was the same as that in the RD sequence. For each subject, pseudo-rotatory stimulus presentations with the fast and slow SOAs were employed in 100 trials, and the total experimental times were nearly 8 min (slow) and 6 min (fast), respectively.

MEG, MRI and fMRI acquisition

To measure the head position in the MEG sensor system, four calibration coils were mounted bilaterally on the temporal skin (two each for the superior superciliary and anterior subauricular regions) of the subjects. Before the MEG recording sessions, the subject's head shape was scanned from three directions (left, right, and front) by using a 3D digital camera (VIVID 700, Konika Minolta, Japan). Electromagnetic calibration of the coil positions was conducted at the beginning of each session by passing alternating currents (19–263 μA, 10 Hz) to the coils. A whole-head 200-channel

MEG system (SBI200, Shimadzu Co., Japan) was used for MEG recordings. The sampling frequency was 1 kHz. A band pass filter (1–100 Hz) and a notch filter were employed. A chin rest was used to avoid movement of the subject's head. Electro-oculograms (EOGs) were simultaneously recorded. Trials whose EOG signal exceeded 75 μV were rejected from further analysis. The MEG signals were collected and averaged for each quadrant in the RD sequence and for each SOA (slow or fast) in the RT sequence.

Structural and functional MR images were obtained with a 1.5-T MR scanner (Shimadzu Marconi, MAGNEX ECLIPSE). Both T1-weighted images (TR=20 ms; TE=2.26 ms; voxel size 1×1×1 mm; matrix size 256×256×191) and EP images (TR=3 s.; TE=55 ms; voxel size 3×3×3 mm; matrix size 64×64×52) covered the whole head of each subject.

Cortical dipole model

A polygon cerebral cortex model for each subject was constructed using FreeSurfer software (Dale et al., 1999) with the T1 structural image for the subject. Although the original polygon model had over 300,000 vertices, these were decimated to one-tenth the number (number of vertices, 34189±1407; inter-vertex distance, 0.5–2.5 mm; Fig. 2a). A cortical dipole model was constructed from the polygon model for each subject by assuming a current dipole at every vertex at which the fMRI activity elicited by any of the four quadrantal stimuli exceeded a threshold (blue dots in Figs. 2a and b). The details of this procedure are described in "FMRI analysis and correct/noisy priors" subsection. This operation reduced the number of dipoles and strongly constrained the inverse solutions in practice. The dipole current directions were assumed perpendicular to the cortical surface. A positive current was defined as one directed toward the inside of the cortex.

The MEG and MRI results were coregistered in three steps. The head shapes obtained from the 3D digital camera and the T1 structural image were fitted by a least-square method, and the calibration coils on the head were registered with respect to the MRI coordinates. Next, the calibration coils were registered with respect to the MEG sensor coordinates by using the electromagnetic calibration (see Kajihara et al., 2004). Finally, combining the above two coordinate transformations, the cortical dipole model in the MRI coordinates was registered with respect to the MEG sensor coordinates. Since the relative sensor positions deviated across sessions (4±2 mm), the sensor positions were averaged across sessions. Under the assumption that electrical conductivity is homogeneous and isotropic inside the skull, the lead fields were calculated by the boundary element method (Mosher et al., 1999; Tissari and Rahola, 2003). The skull shape was extracted from the T1 structural image by using Curry software (Neurosoft Inc., USA).

In this study, we employed the dipole current density, whose unit is [Am/m^2] (Jerbi et al., 2004; Lin et al., 2006), rather than the dipole current (moment), whose unit is [Am]. Accordingly, each component of the lead fields was divided by one-third the sum of the areas of the polygons including the vertex of the corresponding lead field component. For simplicity, however, we refer to the dipole current density as the dipole current in the following sections.

Hierarchical Bayesian estimation

Conventional distributed source methods can impose fMRI information as the prior current variance for each dipole. Consequently, if the fMRI information is not reliable, such methods may give a wrong inverse solution. In the hierarchical Bayesian method, the prior current variance is considered as a random variable, and a hierarchical prior distribution for the

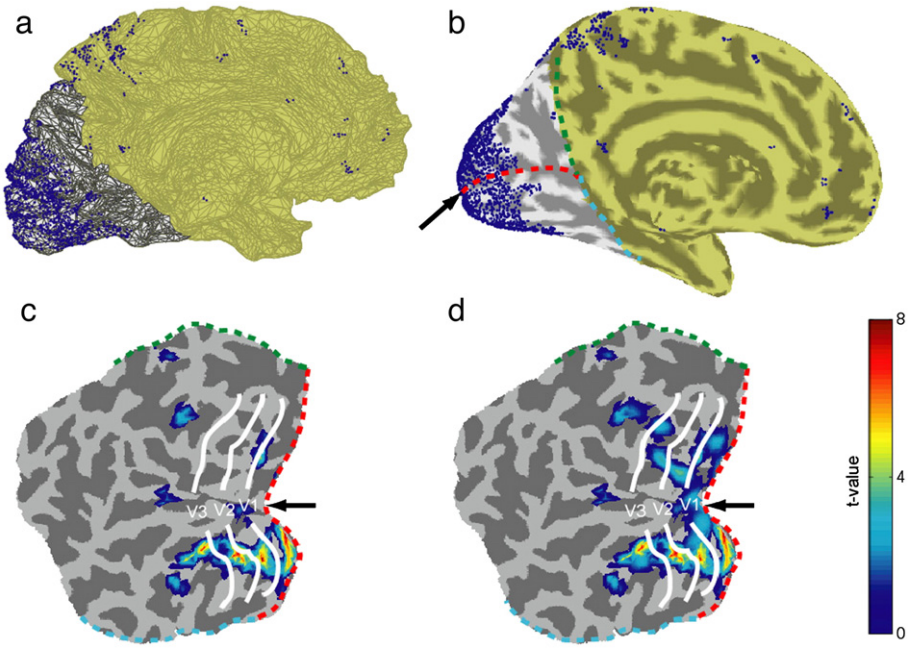

Fig. 2. Cortical surface and fMRI priors. (a) The cortical surface for the left hemisphere of subject 1. The blue dots denote current dipoles at which fMRI activities were observed or artificial activities were added. In the flattened map format, the cortical region filled with light yellow was removed. (b) The same cortical surface in an inflated format. To make the flattened map, the inflated model was cut along the red, green, and cyan dotted lines. (c) The correct prior (fMRI-dipole response) for the UR stimulus in a pseudo-color representation on the flattened map for the left hemisphere of subject 1. The dotted lines correspond to those in (b). (d) The noisy prior corresponding to (c), shown in a pseudo-color representation on the flattened map.

prior current variance is introduced. The fMRI information is imposed on the hierarchical prior through hyperparameters, which are manually chosen before conducting the hierarchical Bayesian estimation. Since the prior current variance is updated according to the observed MEG data, unreliable fMRI information can be compensated to some extent.

The hierarchical prior of an inverse-variance parameter α_i, at the i-th dipole, has a Gamma distribution (Sato et al., 2004), whose mean and degree of freedom are given by $\bar{\alpha}_{0i}$ and γ_{0i}. In the following, we use a current variance parameter $\nu_i \equiv \alpha_i^{-1}$ and $\nu_{0i} \equiv \bar{\alpha}_{0i}^{-1}$, since they have intuitive meaning. These hyperparameters were controlled by two parameters: a variance magnification parameter $m_0(\geq 1)$, and a confidence parameter $\gamma_0(>0)$. The magnification parameter m_0 controls the relative amplitude of the prior current variance. The mean prior current variance, ν_{0i}, was set proportional to the square of the fMRI activity (dipole t-value) and took a value from $\nu_{0,\mathrm{base}}$ to $m_0 \times \nu_{0,\mathrm{base}}$, where $\nu_{0,\mathrm{base}}$ was the baseline current variance estimated by applying a Bayesian minimum norm method to the MEG data before the stimulus onset. Therefore, large m_0 increases the prior current variance, especially for dipoles with large fMRI activities and encourages the estimated current amplitudes become large. It should be noted that the actual prior current variance is given by $\rho \times \nu_i$, where a scaling factor $\rho \times \nu_i$ is the noise variance (see Appendix A). Namely, the calibration constant from fMRI t-value to the current variance is given by $\rho \times m_0$.

The degree of freedom γ_{0i} was set to γ_0 for all dipoles. The confidence parameter γ_0 controls the width of the prior distribution and the variance of the prior distribution was inversely proportional to γ_0. Large γ_0 narrows down the prior distribution around the mean value, and the estimation depends more critically on the fMRI data. When $\gamma_0 \geq 10^5$, in practice, the estimation result becomes almost equivalent to that of the fMRI-weighted minimum norm method. The details of the hierarchical prior and the control of the hyperparameters are described in Appendix A.

When conducting hierarchical Bayesian estimation, a smoothness constraint having a Gaussian profile with a full width at half maximum (FWHM) of 8 mm was incorporated directly into the lead field matrix (see Appendix B). Here, the method of incorporating the smoothness constraint was different from that used in our original model in Sato et al. (2004), in which the smoothness constraint was represented as a hierarchical prior and much computation was required. Instead, we used a simplified method in this study.

For the RD sequence, hierarchical Bayesian estimation was conducted for the MEG data elicited by each quadrantal visual stimulus, with the corresponding fMRI activity as the fMRI prior. For the RT sequence, because of stimulus changes, four retinotopic areas were expected to be activated in a trial. Therefore, the MEG data was divided into 100-ms time windows with 50-ms overlap. Hierarchical Bayesian estimation was conducted for each of divided MEG data under the assumption that the current variance was temporally invariant within each time window. Then, the current variance changed every 50 ms. On the other hand, the current was estimated every 1 ms using the estimated current variance. The prior for each time window was given by the fMRI activity corresponding to the presented stimulus during that time window. In the overlap periods of two time windows, the dipole currents were averaged.

Time and region of interests (TOI and ROI)

The temporal patterns of the dipole currents were analyzed using the time (TOI) and region of interest (ROI), through which the spatial and the temporal patterns of the dipole currents were isolated from each other. These TOI and ROI were determined based on the estimated current dipoles, not fMRI signals. We employed an iterative algorithm to determine the TOI and ROI. First, we globally focused a tentative TOI to the entire peaks of MEG power summed across all sensors and estimated the spatial distribution of the dipole currents averaged across the TOI. Next, a tentative ROI (diameter, 8 mm) was focused on the spatial peak of the temporally averaged dipole currents, and the temporal pattern of the dipole currents was estimated by averaging all dipole currents within the tentative ROI. A fine TOI (duration, 20 ms) was further focused on the temporal peak of the dipole currents estimated through the ROI, and the spatial pattern of the dipole currents was estimated through the fine TOI, and so on. Usually, TOI and ROI converged to the final ones by two or three iterations of this procedure, and they were selected as the TOI and ROI to analyze the spatiotemporal patterns of the dipole currents.

Goodness of estimate measures

Determination of goodness of estimate requires the true brain activity to which the estimates are to be referred. Since the true brain activity underlying MEG is unknown, we selected the activity map of fMRI as the reference to which the hierarchical Bayesian estimates is compared. The spatial coincidence of the dipole currents averaged over a TOI with the activity map of fMRI (i.e., the dipole t-value) was estimated as two goodness of estimate measures.

First, a correlation coefficient between the fMRI activity and the spatial pattern of the dipole current amplitudes was calculated as

$$\mathrm{correlation} = \frac{\sum_{i=1}^{I} J_i \cdot t_i}{\sqrt{\sum_{i=1}^{I} J_i^2 \cdot \sum_{i=1}^{I} t_i^2}}, \tag{1}$$

where I is the number of dipoles, and J_i and t_i denote the temporally averaged current amplitude and the fMRI t-value, respectively, at the i-th dipole. The correlation coefficient is mainly affected by large signals, so it is a good measure for detecting the spatial profile differences in strongly active regions.

Second, a Hamming measure was introduced to detect rather weak false-positive activities. The spatial profiles of the current amplitudes and the fMRI t-values were first thresholded at 10% of the maximum value and converted to binary digits (0 and 1). Then, the Hamming measure between them was calculated as

$$\mathrm{Hamming\ measure} = 1 - \frac{\sum_{i \in K} \tilde{J}_i}{||K||} \quad K = \left\{ i \middle| \tilde{t}_i = 0 \right\}, \tag{2}$$

where $\tilde{J}_i$ and $\tilde{t}_i$ are the binary values for J_i and t_i, respectively. The summation in the second term was taken over the dipoles

with $\tilde{t}_i=0$, and $||K||$ was the number of dipoles in K. In other words, the second term counts the number of false-positive dipoles in regions where the fMRI signal was inactive.

In addition to the spatial pattern of the estimated currents, goodness of fit (GoF) between the observed magnetic field B_n and the magnetic field reconstructed from the estimated current, B'_n, at the time of the first peak of the MEG signal was also calculated as

$$\mathrm{GoF} = 100 \times \left\{ 1 - \frac{\sum_{n=1}^{N} (B_n - B'_n)^2}{\sum_{n=1}^{N} B_n^2} \right\}, \tag{3}$$

where N is the number of MEG sensors, and n is the sensor index.

To investigate the effect of the hyperparameters on the temporal patterns of estimated dipole currents, we calculated the current-space GoF (CGoF) as

$$\mathrm{CGoF} = 100 \times \left\{ 1 - \frac{\sum_\tau (J(\tau) - J_{\mathrm{ref}}(\tau))^2}{\sum_\tau J_{\mathrm{ref}}^2(\tau)} \right\}, \tag{4}$$

where $J_{\mathrm{ref}}(\tau)$ is the temporal pattern of the reference estimate, and $J(\tau)$ is the temporal pattern of the dipole currents to be evaluated. These temporal patterns were calculated by averaging all dipole currents in a ROI. The temporal summations of the right-hand side in Eq. (4) were taken in a TOI.

Measures for estimated variance parameters

As described in "Hierarchical Bayesian estimation" subsection, the variance magnification parameter m_0 is the ratio between the maximum of the mean prior current variance ν_{0i} to the baseline current variance $\nu_{0,\mathrm{base}}$. Since the variance magnification parameter is a scaling factor for the variance parameter, one might consider that the current density must be known in order to determine the value of the variance magnification parameter value before estimation.

To examine the effect of m_0 on hierarchical Bayesian estimation, we calculated the following two quantities. One is the prior variance ratio:

$$\max_i \left(\frac{\nu_i}{\nu_{0,\mathrm{base}}} \right), \tag{5}$$

which is the ratio of the maximum of the variance parameter value to the baseline value. The other is the current variance ratio:

$$\frac{\max_i \mathrm{var}(J_i)}{\rho_{\mathrm{base}} \cdot \nu_{0,\mathrm{base}}}, \tag{6}$$

which is the ratio of the maximum of the dipole current variance to the baseline of the prior current variance. The dipole current variance is defined by

$$\mathrm{var}(J_i) = \frac{1}{T} \sum_\tau \left[J_i(\tau) - \bar{J}_i \right]^2, \quad \bar{J}_i = \frac{1}{T} \sum_\tau J_i(\tau). \tag{7}$$

$\nu_{0,\mathrm{base}}$ and ρ_{base} were estimated by applying a Bayesian minimum norm method to the MEG data before the stimulus onset.

Results

fMRI analysis and correct/noisy priors

The fMRI signals elicited by the four quadrantal stimuli were analyzed using SPM2 (Wellcome Department of Cognitive Neurology, UK) and mapped to the MRI voxels after correcting for the slice times and head motions. The voxel t-values for the difference between the stimulus and the rest conditions ($p<0.001$, uncorrected) were mapped to the cortical vertices by using a Gaussian mapping function (FWHM=5 mm, see Kajihara et al., 2004). The mapped t-values were smoothed with a step function with an 8-mm diameter along the cortical surface.

Fig. 2c shows a pseudo-color representation of the fMRI response profile on the cortical surface elicited by the UR stimulus for subject 1 in a flattened map format (Sereno et al., 1995). The flattened map was made by cutting along the bottom of the calcarine sulcus (Fig. 2b, red dotted line). Four stripe activities were observed in parallel on the lower part of the calcarine sulcus in the left hemisphere, corresponding to the UR stimulus. These activities approximately corresponded to V1, V2, V3, and V4, starting from the calcarine sulcus. Small activities were also observed close to the V1/V2 border of the upper side of the calcarine sulcus, the lateral occipital cortex (LOC) of the left hemisphere, and the superior parietal sulcus (SPS) of both hemispheres. Since the V2 and V3 fMRI activities were not clearly separated in 14 of 16 cases (four subjects, four quadrants), we combined the V2 and V3 activities in analyzing of the spatiotemporal brain activities estimated from the MEG data.

For three of the four subjects, fMRI activities were observed in the early visual areas (V1–V3) for the four visual quadrant stimuli as well as in Fig. 2c, although there were no activities in the LOC and SPS in half of the cases. For the one remaining subject, the UL stimulus elicited strong responses anterior to the early visual areas, near the ventral occipital cortex, and the V1 response was very weak. Consequently, we ruled out the MEG data for this case and analyzed the 15 remaining cases.

In six of these cases (five upper and one lower quadrant), the V4 activities were very weak. Therefore, we ruled these six cases out of our analysis of the V4 activity estimated from the MEG data. V4 has a retinotopically organized hemifield; that is, the anterior and posterior parts represent the upper and lower quadrants, respectively (Brewer et al., 2005). Although our fMRI experiments revealed activities around V4 caused by stimulus presentation in the upper and lower quadrants in the remaining nine cases, no clear retinotopic organizations was observed.

We chose cortical vertices that exhibited significant fMRI activities ($p<0.1$) and constructed a prior for each subject and each stimulus. We refer to this as the "correct prior" (essentially the same as the fMRI t-value, as shown in Fig. 2c). We also constructed a noisy prior by adding 20 artificial activities with an 8-mm diameter (along the cortical surface) and SN=2 (i.e., half the maximal fMRI activity) to each correct prior. The center vertices of the artificial activities were pseudo-randomly chosen from the cortical vertices within 50 mm from the occipital pole, while requiring that the vertices be at least 8 mm (in Euclidean distance) from each other. Fig. 2d shows the noisy prior corresponding to the correct prior shown in Fig. 2c. In addition to the fMRI activities appearing in the correct prior, weak false activities were also observed in the occipital cortex

and spreading out from V1 to V4 and the LOC, including the upper and lower sides of the calcarine sulcus. A cortical dipole model was constructed for each subject according to the above priors. Namely, dipoles were assumed on the union of the four fMRI active areas and the artificial active areas (2567–4429 dipoles; blue dots in Fig. 2a).

MEG data

Fig. 3a shows the global field power (GFP, the sum of all MEG sensor signal amplitudes) recorded from subject 1's responses elicited by the UR stimulus. The first strong peak was observed 95 ms after the stimulus onset, followed by a strong peak at 202 ms with almost the same amplitude. In all 15 cases, the first peak of the GFP was observed at around 100 ms (105.2 ± 12.1 ms). In 13 of 15 cases, the first peak was followed by a single peak (eight cases) or double peaks (five cases) within 150–300 ms. The latencies of the second and third peaks varied significantly (174.3 ± 34.8 ms for the second, 221.2 ± 39.2 ms for the third). The remaining two cases did not have any significant peaks after the first one and showed sustained time courses.

Hierarchical Bayesian estimation with fMRI constraint

We conducted hierarchical Bayesian estimation with the correct priors using a reference set of hyperparameters, $\gamma_0 = 500$, $m_0 = 500$ and studied the effects of deviation of the two hyperparameters from the reference on the hierarchical Bayesian estimates. Fig. 3 shows a representative brain activity thus estimated (subject 1 for UR stimulus). The tentative TOI was focused on the period (50–300 ms) including all peaks of the MEG signal (Fig. 3a, dashed line). This tentative TOI was also used to calculate goodness measures (correlation coefficient and Hamming measure). The ROI (diameter, 8 mm) was focused on the peak brain activities localized in the known regions of V1, V2/3 or V4. The fine TOI (20 ms) was focused on the first peak of dipole currents in each region.

Figs. 3b, e–g show the spatiotemporal patterns of the estimated dipole currents. Within the earliest TOI (93 ± 10 ms), the strongest activity was observed at V1 (Fig. 3e). The temporal pattern (blue trace in Fig. 3b) of the V1 ROI (blue ellipse in Fig. 3e), which started 60 ms after the stimulus onset as a positive current, attained the first peak at 93 ms, after which the current direction was reversed. Then, the second peak was observed at 168 ms, and the activity gradually decreased. Within the second TOI (98 ± 10 ms), a strong activity had a peak in the V2/3 region (Fig. 3f). The temporal pattern (green trace in Fig. 3b) of the V2/3 ROI (green ellipse in Fig. 3f) started slightly later (72 ms for the onset, 98 ms for the peak) than that of the V1 ROI, but it attained almost the same amplitude and exhibited a similar temporal pattern. Within the third TOI (134 ± 10 ms), an activity with a medium amplitude was observed in V4. The temporal pattern (red trace in Fig. 3b) of the V4 ROI (red ellipse in Fig. 3g) had basically the same characteristics as those for V1 and V2/3, although the amplitude was relatively weak as compared to V2/3, the onset and peak time were relatively later (86 ms and 132 ms, respectively), and the second peak was not observed.

Figs. 3c and i show the spatiotemporal patterns of the dipole currents estimated with the noisy prior and the reference hyperparameters. The ROIs in Fig. 3i are the same as those in

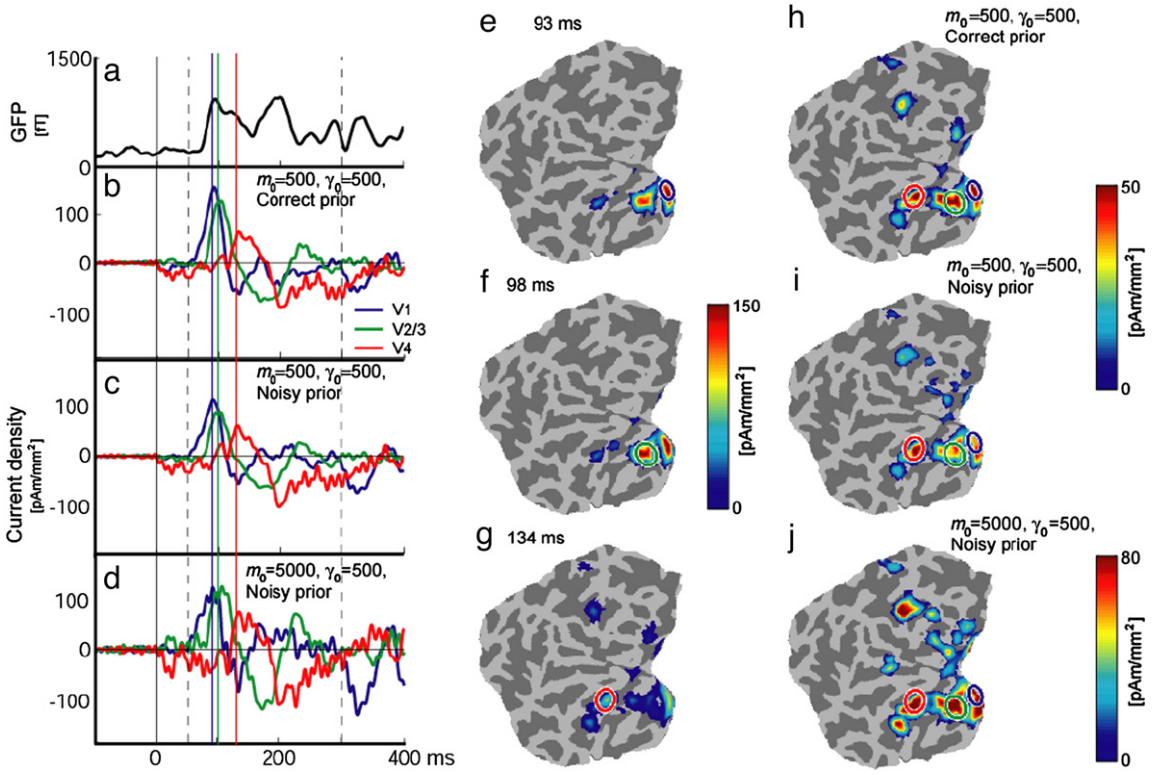

Fig. 3. MEG signals elicited by the UR stimulus presentation and spatiotemporal patterns of the dipole currents estimated with fMRI constraint, for subject 1. (a) The temporal pattern of the global field power (GFP). (b, h) The temporal (b) and spatial (h) patterns of the dipole currents estimated with the correct prior and the reference hyperparameter values ($\gamma_0 = 500$, $m_0 = 500$). The three ROIs (V1, V2/3, and V4) are represented by the red, green, and blue ellipses on the flattened map. (e–g) Spatial patterns of the estimated dipole currents are illustrated with the three TOIs corresponding to the three ROIs. (c, i) The temporal (c) and spatial (i) patterns of the dipole currents estimated with the noisy prior and the reference hyperparameter values. (d, j) The temporal (d) and spatial (j) patterns of the dipole currents estimated with the noisy prior and a large m_0 ($\gamma_0 = 500$, $m_0 = 5000$).

the correct-prior case (Fig. 3h). Rather weak false-positive activities, corresponding to the artificial activities in the noisy prior, were observed on the upper side of the calcarine sulcus (Fig. 3i). However, the temporal patterns of V1, V2/3 and V4 (Fig. 3c) were very similar to those for the correct-prior case (Fig. 3b), although their amplitudes were slightly weaker. These observations indicate that the hierarchical Bayesian method employing the reference hyperparameters is tolerant with respect to false-positive activities.

Effect of hyperparameters

We further investigated the effect of the hyperparameters on the estimation results by varying the hyperparameter values. In the above case (subject 1, UR stimulus), a large γ_0 (m_0=500, γ_0=5000) with the correct prior did not affect the spatiotemporal pattern of the estimated dipole currents. On the other hand, a large m_0 (m_0=5000, γ_0=500) increased the dipole current amplitudes by a factor of 1.5 times in all ROIs for V1–V4, although the spatial patterns and the shapes of the temporal patterns were almost the same as those for the reference hyperparameters (result not shown).

With the noisy prior, large γ_0 slightly increased the false-positive activities but did not significantly affect the temporal patterns of the ROIs for V1–V4 ROIs (not shown). Large m_0 increased the dipole current amplitudes by a factor of 1.7 times in all ROIs, as in the correct-prior case, and resulted in prominent false-positive activities (Fig. 3j) and noisy temporal patterns in the three ROIs (Fig. 3d).

We also evaluated the effect of hyperparameter changes for the other 14 cases and obtained essentially the same results for all 15 cases. The increase factors of the dipole current amplitudes for large m_0, averaged over the 15 cases, were 1.81 ± 0.15 and 2.42 ± 0.84 for the correct and noisy priors, respectively. The tolerance for noisy priors was confirmed in 10 of 15 cases with the reference hyperparameters, although rather weak false-positive activities appeared in 5 of 10 cases.

Retinotopy in quadrantal visual stimulation

Fig. 4 shows the estimated spatiotemporal activities in the occipital cortices of subject 2, for the four quadrantal visual stimuli, with the correct priors and the reference hyperparameters. For the LL (Fig. 4c) and UL stimuli (Fig. 4d), V1, V2/3, and V4 were sequentially activated as in the case of the UR stimulus for subject 1 (Fig. 4b). V4 activities for the upper (UL) and lower (LL) stimuli were observed in almost the same area, but retinotopic organization was not identified within V4. For the UR stimulus (Fig. 4a), the early visual areas were also sequentially activated, but the amplitude of the V1 activity was relatively weak. Furthermore, the peak latencies for V2/3 and V4 were about 10 ms later and about 10 ms earlier,

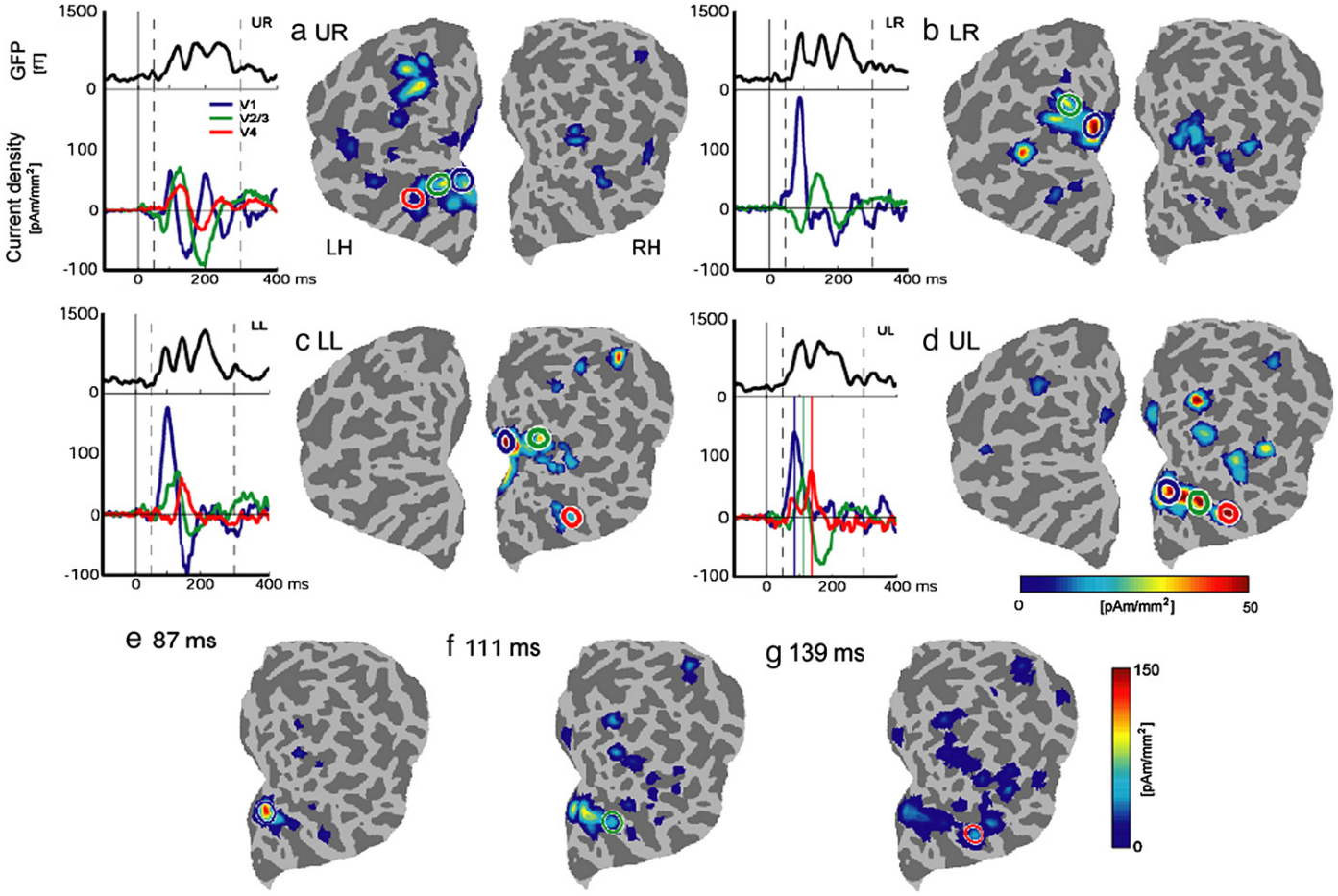

Fig. 4. GFP of the MEG signals elicited by the four visual quadrant stimuli, UR (a), LR (b), LL (c), and UL (d), presented to subject 2, and the spatiotemporal patterns of the dipole currents in the three ROIs, estimated with correct priors and the reference hyperparameter values. The spatial patterns calculated through the tentative TOI for the four visual quadrant stimuli are represented in the flattened map format. (e–g) Spatial patterns of the estimated dipole currents for the UL stimulus are illustrated with the three TOIs corresponding to V1, V2/3, and V4 ROIs.

respectively, than those for the UL and LL stimuli. For the LR stimulus (Fig. 4b), the V1 and V2/3 activities were also sequentially activated, while the V4 activity was very weak. Therefore, we discarded the V4 activity from the analysis (not shown in the figure). In addition, the V2/3 activity started with a weak negative response. This seems to be crosstalk between the V1 and V2/3 currents and might be explained by the high correlation (0.83) between the lead fields corresponding to the dipoles at the centers of these ROIs.

The above analyses showed that brain activities elicited by quadrantal visual stimuli were retinotopically localized. To show the spatiotemporal brain activities in detail, we focused TOI/ROIs on the spatiotemporal peaks of brain activities in V1, V2/3, and V4 for the UL stimulus (Figs. 4e–g). The center of these TOIs corresponds to the blue, green, and red vertical lines in the lower left graph of Fig. 4d. As in the case shown in Figs. 3e–g, spatial patterns of cortical activities within three TOIs (87, 111, and 139 ms) had peaks in V1, V2/3 and V4, respectively, and the strongest activity was observed in V1. The temporal patterns of estimated currents in the three ROIs showed a sequential activation that started with positive currents. However, reversals in dipole current direction, as shown in Fig. 3b, were not observed in temporal patterns in V1 and V4 ROIs.

Here, we summarize the spatiotemporal patterns for all 15 cases with correct priors and the reference hyperparameters. In all 15 cases, the V1 activities exhibited similar temporal patterns to that of the UR case for subject 1 and revealed retinotopic responses, comparable to the retinotopic maps reported by fMRI studies of the human V1 (Sereno et al., 1995; Tootell et al., 1997). In five cases, however, the V2/3 activities exhibited crosstalks in the temporal pattern, as in the LR case for subject 2. In six cases, the V4 activities were very weak, and these V4 activities were discarded. The mean peak latencies of the early visual areas were calculated without these uncertain cases (93.6±3.9 ms for V1, 110.4±12.0 ms for V2/3, 130.7±16.0 ms for V4). These results roughly agree with previous MEG/EEG studies using pattern onset stimuli (Di Russo et al., 2001; Kajihara et al., 2004; Vanni et al., 2004). In addition, the current densities in the V1 ROI at the first peak of each time course (194.2±60 pAm/mm^2) roughly matched with previous electrophysiological studies (between 25 and 250 pAm/mm^2; briefly summarized in Jerbi et al., 2004).

Proper range of hyperparameters

The above observations indicate that estimation results using real MEG, MRI, and fMRI data depend on the hyperparameters. Even if correct priors are used, the proper range of hyperparameters is limited by the many factors described in the Introduction. To investigate the effect of the hyperparameters and evaluate their proper range, we varied γ_0 and m_0 over the ranges of 0.01–10^{10} and 1–10,000, respectively, and evaluated the subsequent estimation results.

Correct prior

We evaluated the proper range of the hyperparameters for correct priors by goodness measures described in "Materials and methods" section. Fig. 5a shows a pseudo-color plot of the correlation coefficient, averaged over the 15 cases of estimation results employing correct priors, with respect to γ_0 and

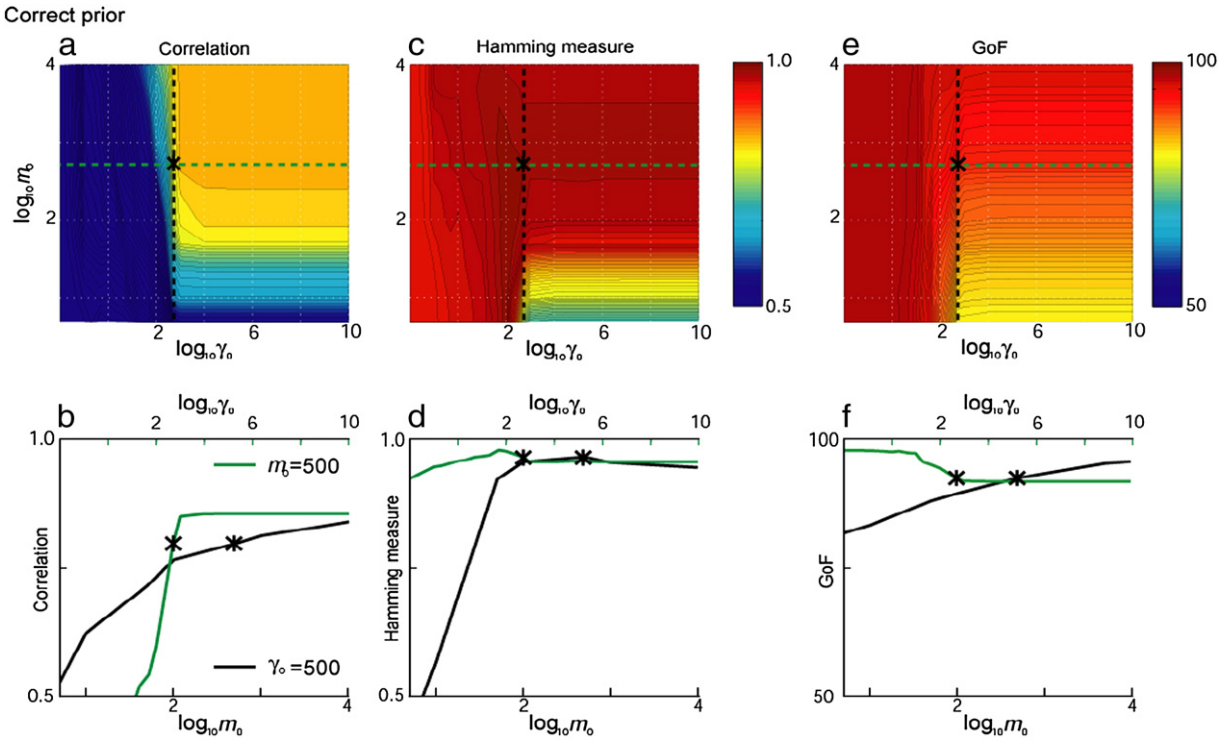

Fig. 5. Correlation coefficient, Hamming measure, and GoF with respect to γ_0 and m_0. The hierarchical Bayesian estimation was conducted with correct priors. Each plot is the average of 15 cases. (a) The correlation coefficient between the spatial pattern of the estimated dipole currents and the correct prior is shown in a pseudo-color representation. The asterisk denotes the reference hyperparameter values. (b) The profiles of the correlation coefficient across the reference hyperparameters. The green and black traces correspond to the reference values of m_0 and γ_0, respectively. Note that the two traces have different scales for the abscissa. The upper and lower scales correspond to the green and black traces, respectively. (c–f) The Hamming measure (c, d) and GoF (e, f) are represented in the same format as for the correlation coefficient (a, b).

m_0. The correlation coefficient was positively correlated with both γ_0 and m_0. Fig. 5b shows profiles of the correlation coefficient with respect to γ_0 (green trace) and m_0 (black trace), along with the reference values of m_0 and γ_0 (asterisks). The correlation coefficient increased abruptly with γ_0 in the medium range ($100 \leq \gamma_0 \leq 1000$) and was almost flat in the low-γ_0 range ($\gamma_0 \leq 100$) and the high-γ_0 range ($\gamma_0 \geq 1000$). On the other hand, the correlation coefficient rapidly increased in the low-m_0 range ($m_0 \leq 100$) and gradually increased in the medium- ($100 \leq m_0 \leq 1000$) and high-m_0 ($m_0 \leq 1000$) ranges.

Figs. 5c and d show a pseudo-color plot of the Hamming measure (averaged over the 15 cases) and its profiles with respect to γ_0 (green trace) and m_0 (black trace), respectively. Compared with the correlation coefficient, the Hamming measure showed weak dependency on γ_0 in the medium- and high-m_0 ranges. The profile with respect to γ_0 showed a slight increase from the low to the medium range, attained a peak near $\gamma_0 = 100$, slightly decreased in the medium range, and became almost flat in the high range. The dependency on m_0 was rather strong as compared with that of the correlation coefficient. The profile with respect to m_0 showed a rapid increase from the low to the medium range, attained a peak near the reference value (asterisk), and slightly decreased in the high range.

Figs. 5e and f show a pseudo-color plot of the GoF (averaged over the 15 cases) and its profiles with respect to γ_0 (green trace) and m_0 (black trace), respectively. Compared to the correlation coefficient and the Hamming measure, the GoF exhibited weak dependencies on γ_0 and m_0. It decreased with γ_0 in the low and medium ranges and was almost flat from the medium to the high range. In contrast, the GoF increased slightly in all ranges with respect to m_0. Regardless of γ_0, it was higher than 90% in the medium- and high-m_0 ranges.

In addition to evaluating the GoF, we also investigated the characteristics of the free energy, which is a criterion indicating how well observed data were explained by a given statistical model (Sato et al., 2004). The free energy had characteristics similar to those of the GoF (not shown).

With the correct prior, both of the correlation coefficient and the Hamming measure exhibited high values in the medium and high ranges of γ_0 and m_0 (Table 1). The GoF was also sufficiently high in the medium and high ranges of γ_0 and m_0, although it achieved its highest values in the low-γ_0 range. These observations indicate that good estimates were obtained in the medium and high ranges of γ_0 and m_0.

Table 1
Summary of hyperparameter range analysis

	Low γ_0	Medium γ_0	High γ_0
a. Correct prior			
High m_0	Corr: 0.36±0.22	Corr: 0.66±0.29	Corr: 0.73±0.30
	Hamm: 0.96±0.03	Hamm: 0.95±0.07	Hamm: 0.94±0.07
	GoF: 97.3±1.74	GoF: 96.0±2.31	GoF: 95.6±2.44
Medium m_0	Corr: 0.31±0.17	Corr: 0.63±0.29	Corr: 0.72±0.29
	Hamm: 0.95±0.05	Hamm: 0.96±0.05	Hamm: 0.95±0.06
	GoF: 96.9±2.07	GoF: 92.0±5.20	GoF: 91.1±5.27
Low m_0	Corr: 0.17±0.12	Corr: 0.44±0.26	Corr: 0.54±0.26
	Hamm: 0.94±0.03	Hamm: 0.69±0.32	Hamm: 0.52±0.28
	GoF: 72.2±41.8	GoF: 63.2±37.3	GoF: 61.0±36.0
b. Noisy prior			
High m_0	Corr: 0.25±0.20	Corr: 0.48±0.26	Corr: 0.55±0.24
	Hamm: 0.95±0.04	Hamm: 0.84±0.10	Hamm: 0.79±0.08
	GoF: 96.8±1.66	GoF: 95.5±2.27	GoF: 95.3±2.41
Medium m_0	Corr: 0.22±0.16	Corr: 0.48±0.27	Corr: 0.59±0.25
	Hamm: 0.95±0.03	Hamm: 0.90±0.09	Hamm: 0.84±0.07
	GoF: 96.3±2.06	GoF: 92.4±4.98	GoF: 91.3±5.79
Low m_0	Corr: 0.14±0.11	Corr: 0.39±0.24	Corr: 0.48±0.24
	Hamm: 0.95±0.03	Hamm: 0.68±0.31	Hamm: 0.50±0.26
	GoF: 71.6±41.5	GoF: 63.5±37.5	GoF: 61.8±36.5

Corr = correlation; Hamm = Hamming measure; GoF = goodness of fit.

Noisy prior

We also evaluated the proper range of the hyperparameters for noisy priors. Figs. 6a and b show a pseudo-color plot of the correlation coefficient and its profiles with respect to γ_0 and m_0. The characteristics of the correlation coefficient with respect to γ_0 were similar to those for the correct-prior case, although the actual values were rather low in all ranges. The correlation coefficient was very low in the low-γ_0 range, abruptly increased to a peak value in the medium range, and was almost flat in the high-γ_0 range. With regard to m_0, the correlation coefficient gradually increased from the low to the medium range, then decreased from the medium to the high range.

The Hamming measure slightly increased from the low- to the medium-γ_0 range, attained a peak near $\gamma_0 = 100$, followed by a rapid decrease, and maintained a low value in the high range (Figs. 6c and d). With regard to m_0, the Hamming measure rapidly increased from the low to the medium range, attained a peak near the reference value, and slightly decreased in the high range. The GoF profiles (Figs. 6e and f) were almost the same as in the correct-prior case, and the GoF was higher than 90% in the medium- and high-m_0 ranges, regardless of γ_0.

With the noisy prior, good estimates in terms of the correlation coefficient were obtained in the medium- and high-γ_0 ranges and in the medium-m_0 range. Good estimates in terms of the Hamming measure were obtained in the low- and medium-γ_0 ranges and in the medium- and high-m_0 ranges. Considering the intersection of the proper ranges with respect to both the correlation coefficient and the Hamming measure, the medium-γ_0 and -m_0 ranges are reasonable. These ranges are also included in the proper ranges for the correct prior. In addition, the GoF values were sufficiently high (≥90%) and the reference hyperparameter values are included in the medium ranges.

Hierarchical Bayesian estimation without fMRI constraint

The dipole currents for the four quadrantal visual stimuli presented in the RD sequence were estimated without fMRI constraints. Current dipoles were assumed on the whole cortex, unlike the case when fMRI information was employed. A confidence parameter value $\gamma_0 = 10$, which was used in Nummenmaa et al. (2007b), was employed. Mean prior current variances were assumed to have a uniform spatial pattern, i.e., all dipoles have the same value, $\bar{v}_{0i} = m_0 \times v_{0,\mathrm{base}}$, with a variance magnification value $m_0 = 100$.

Figs. 7b and c show the estimated brain activities for subject 1, elicited by the UR stimulus. Single current source was estimated in V2 region and other regions were not activated across the whole time period. Indeed, the estimated prior current variance for the current source was significantly larger than those for other current dipoles. The temporal pattern of a ROI (blue ellipse in Fig. 6c) attained the first peak at 95 ms after the stimulus onset. After that, the current direction was reversed. The latency of the first peak was consistent with the time course of the GFP of the MEG signal.

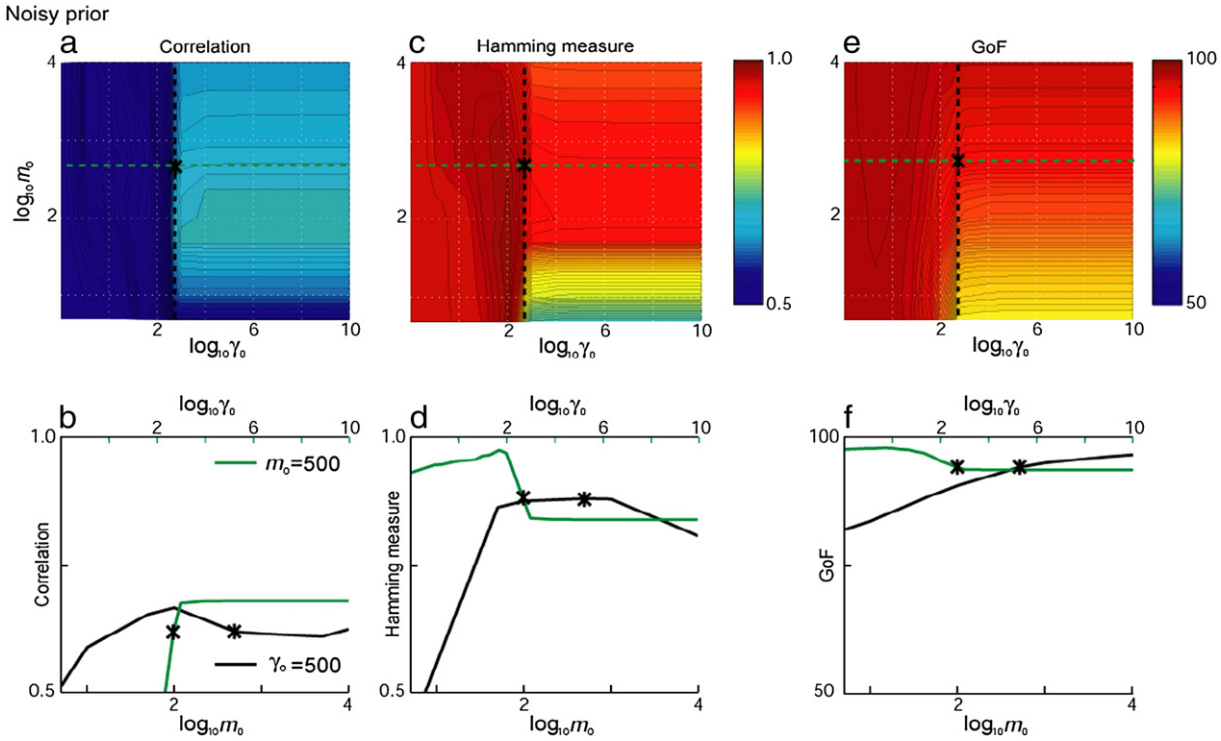

Fig. 6. Correlation coefficient, Hamming measure and GoF with respect to γ_0 and m_0. The hierarchical Bayesian estimation was conducted with noisy priors. Each plot is the average of 15 cases. The correlation coefficient (a, b), Hamming measure (c, d) and GoF (e, f) are shown in the same formats as in Fig. 5.

When fMRI constraint was not imposed, estimated brain activities were sparse; a small number of current sources (at most 6) were estimated for all 15 cases. Some of estimated current sources were far from early visual areas (V1, V2/3, and V4), although always located in the occipital cortex. The distance of current sources from the occipital pole was 3.02 ± 1.07 cm. In Figs. 5 and 6, the bottom line corresponds to the above uniform prior with m_0=1, although current dipoles were limited to the visual areas. The hierarchical Bayesian estimation with such hyperparameter values resulted in low correlation coefficient and Hamming measures as shown Figs. 5 and 6.

In sum, even when fMRI information is not available, brain activities are roughly estimated. However, fine spatiotemporal resolution of brain activities cannot be achieved in realistic situations.

Evaluation of temporal pattern of estimated currents

The correlation coefficient and the Hamming measure are criteria with respect to the spatial pattern of the dipole currents. The hyperparameters, however, affect not only the spatial pattern but also the temporal pattern of the dipole currents, as shown in Fig. 3d. We thus investigated the variation of the temporal pattern with respect to systematic changes in γ_0 and m_0 from the reference values. The dipole current responses were estimated with five combinations of γ_0 and m_0: the reference values for both (γ_0=500, m_0=500), a small γ_0 (γ_0=50, m_0=500), a large γ_0 (γ_0=10^5, m_0=500), a small m_0 (γ_0=500, m_0=50) and a large m_0 (γ_0=500, m_0=5000). We focused on three ROIs (V1, V2/3, and V4), which were determined by the same procedure described previously. Figs. 8a–c show the temporal patterns of the V1,

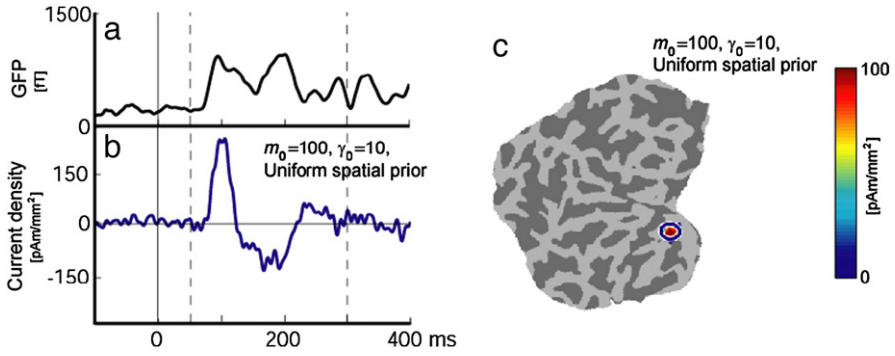

Fig. 7. MEG signals elicited by the UR stimulus presentation and spatiotemporal patterns of the dipole currents estimated without fMRI constraint, for subject 1. (a) The temporal pattern of the global field power (GFP). (b, c) The temporal (b) and spatial (c) patterns of the dipole currents estimated with the uniform spatial prior and hyperparameter values γ_0=10, m_0=100. The spatial pattern was calculated as a temporal average of the dipole current amplitudes over the tentative TOI (50–300 ms after stimulus onset).

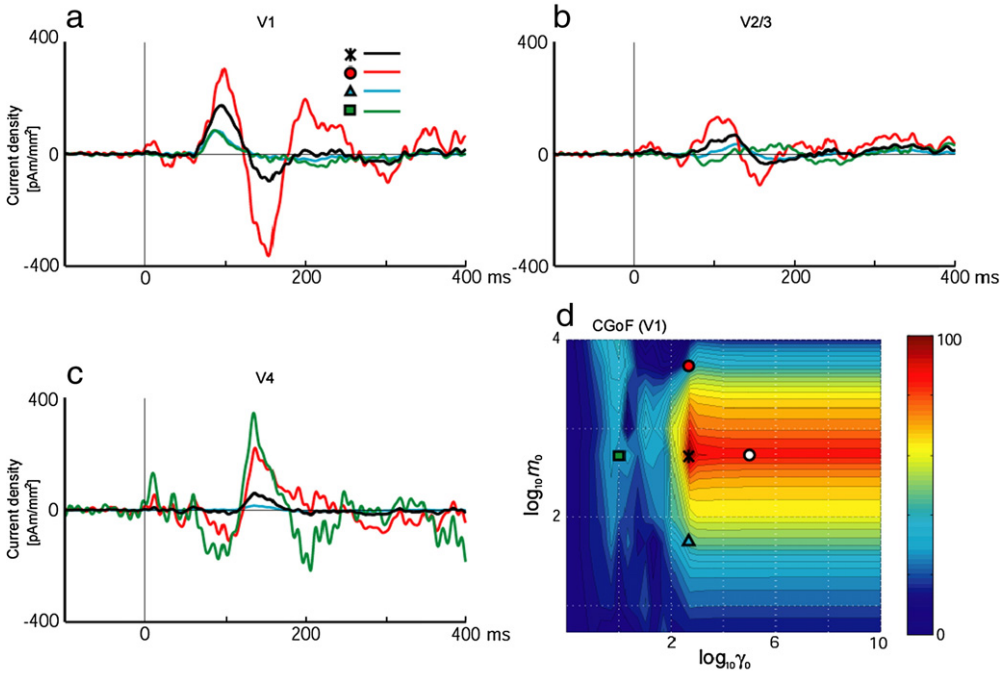

Fig. 8. Effect of the hyperparameters on the temporal pattern of the dipole currents. (a–c) Temporal patterns of the dipole currents (for subject 2 with stimulus LL) in three ROIs (V1, V2/3, and V4), estimated with the correct prior and four combinations of hyperparameters (reference, small/large m_0, small γ_0). For large γ_0, the time course almost overlapped with those for the reference hyperparameter values, so this case is omitted in these figures. (d) Plot of the current-space GoF (CGoF) in a pseudo-color representation. The five marks correspond to the five combinations of γ_0 and m_0.

V2/3, and V4 responses of subject 2 to the LL stimulus, estimated with the five combinations of parameter sets and the correct prior.

The responses for the reference values were the same as those shown in Fig. 4c. For small γ_0 (green traces in Figs. 8a–c), the V1 and V2/3 responses decreased by half, while the V4 response increased by a factor of 5 and exhibited a spurious negative peak. The increases or decreases in the V1, V2/3, and V4 responses, however, were not consistent among the 15 cases, and no systematic changes in the three ROIs were observed. For large γ_0, there was no significant change in the temporal patterns for all 15 cases (not shown). For the small m_0 (cyan traces in Figs. 8a–c), the V1 and V2/3 responses decreased by half, and the V4 response almost vanished. The amplitudes in the three ROIs decreased in all 15 cases, and the mean decrease in the amplitudes averaged over the 15 cases and the three ROIs with TOI = 50–150 ms was by a factor of 0.66 ± 0.49. For large m_0 (red traces in Figs. 8a–c), the amplitudes of the V1 and V2/3 responses increased by a factor of 2, and the V4 response increased by a factor of 4. In addition, spurious peaks were observed in the time courses of the V1, V2/3, and V4 responses. The amplitudes in the three ROIs increased in all 15 cases, with a mean increase by a factor of 1.36 ± 0.52.

When employing the noisy prior, the temporal patterns for the reference hyperparameters did not show much difference as compared to those in the correct-prior case. The effects of changes in γ_0 and m_0 were almost the same as those in the correct-prior case. The mean decrease and increase in the amplitudes averaged over the 15 cases and the three ROIs with TOI = 50–150 ms were by respective factor of 0.70 ± 0.46 and 1.1 ± 0.40, for small and large m_0, respectively.

Fig. 8d shows a pseudo-color plot of the CGoF (averaged over the 15 cases) for correct priors, calculated using the V1 ROI (diameter, 8 mm) and TOI = 50–150 ms. The CGoF exhibited quite small values in the low-γ_0 range, regardless of m_0. In the medium- and high-γ_0 ranges, the CGoF was strongly dependent on m_0. The CGoF attained high values in the medium-m_0 range but had low values in the low- and high-m_0 ranges. CGoF values for individual cases showed similar characteristics to the average values in the medium- and high-γ_0 ranges. In all 15 cases, the CGoF attained high values in the medium-m_0 range and took low values in the low- and high-m_0 ranges, as in the average case. Furthermore, in the medium range of m_0 and γ_0 ($100 \le m_0$, $\gamma_0 \le 1000$), the CGoF was not much varied across individual cases compared to those in the other hyperparameter ranges. Actually, the average of the standard deviation values across the whole range of hyperparameter values was 29.3, while the average across the medium range was 17.1. In the low-γ_0 range, CGoF values for individual cases were lower than those in the medium- and high-γ_0 ranges, but there were no common characteristics. When employing the noisy prior, the CGoF showed characteristics similar to those in the correct-prior case (not shown).

The above observation indicates that the temporal patterns are robust in the medium- and high-γ_0 ranges together with the medium-m_0 range, regardless of the prior employed. On the other hand, the temporal patterns change their amplitudes and shapes very much in the low- and high-m_0 ranges and the low-γ_0 range. The above findings also confirm that the medium-γ_0 and medium-m_0 ranges are appropriate for hierarchical Bayesian estimation.

Variance magnification parameter and current variance

The square root of the baseline of the prior current variance, $(\rho_{\text{base}} \times \nu_{0,\text{base}})^{1/2}$, averaged over the 15 cases, was

Table 2
Prior variance ratio and current variance ratio (HB: hierarchical Bayesian method; MN: minimum norm method)

	HB	HB	HB	HB	MN
	$m_0=500$ $\gamma_0=500$	$m_0=5000$ $\gamma_0=500$	$m_0=50$ $\gamma_0=500$	$m_0=100$ $\gamma_0=10$	
$\max_i\left(\frac{\nu_i}{\nu_{0,\mathrm{base}}}\right)$	514.0	4.97×10^3	89.4	4.38×10^4	371.2
$\frac{\max_i \mathrm{var}(\boldsymbol{J}_i)}{\rho_{\mathrm{base}}\cdot\nu_{0,\mathrm{base}}}$	107.7	334.1	44.5	225.0	41.8

Note that in MN, a_i takes the same value for all current dipoles, while $\boldsymbol{J}_i$ can vary. The values in the table are the averages of 15 cases.

8.9 pAm/mm^2. ν_i and J_i were estimated under the following conditions: (1) by the hierarchical Bayesian method (HB) with the reference hyperparameters ($\gamma_0=500$, $m_0=500$); (2) by HB with large m_0 ($\gamma_0=500$, $m_0=5000$); (3) by HB with small m_0 ($\gamma_0=500$, $m_0=50$); (4) by HB with the uniform spatial prior ($\gamma_0=10$, $m_0=100$); and (5) by the Bayesian minimum norm method (MN). Table 2 summarizes these quantities.

When fMRI information was imposed ($\gamma_0=500$; case (1), (2), and (3)), the prior variance ratios were nearly equal to m_0. Such small differences imply the effect of the hierarchical Bayesian estimation. On the other hand, the current variance ratios were not proportional to m_0. For the reference hyperparameters, the current variance ratio (107.7) was of the same order as m_0 (500). Note that the increase in the current variance ratio for large m_0 (5000) as compared to small m_0 (50) was by a factor of 7.5, which is much smaller than the ratio of the variance magnification parameter values (100). This result indicates that the hierarchical Bayesian method is not especially sensitive to the variance magnification parameter, because the amplitude of the estimated current is constrained such that the MEG signal is well reconstructed. Consequently, delicate tuning of the variance magnification parameter is not required.

When employing the reference hyperparameters, the prior variance ratio was relatively close to that for the MN case (514.0 and 371.2). On the other hand, the current variance ratio was about two times larger than that for MN. We consider this difference plausible. The Bayesian minimum norm method assumes the same value of the prior current variance for all dipoles, while in the hierarchical Bayesian method, the prior current variances depend on fMRI activities. As a result, the current variance of the dipole with the maximal fMRI activity became much larger than those of the current variances of the other dipoles.

When using the uniform spatial prior, the prior and current variance ratios were much larger than those for the reference hyperparameters. The spatiotemporal peak of the current amplitude (405.9±214.6 pAm/mm^2) was relatively larger than that with the reference hyperparameters (286.1±92.4 pAm/mm^2). Indeed, the number of significantly activated dipoles was much smaller than that with the reference hyperparameters.

Effect of constraint on dipole location

As shown in Fig. 2b, current dipoles were limited to the visual cortex. Therefore, it is possible that MEG signal, originally elicited by regions outside the visual cortex, was

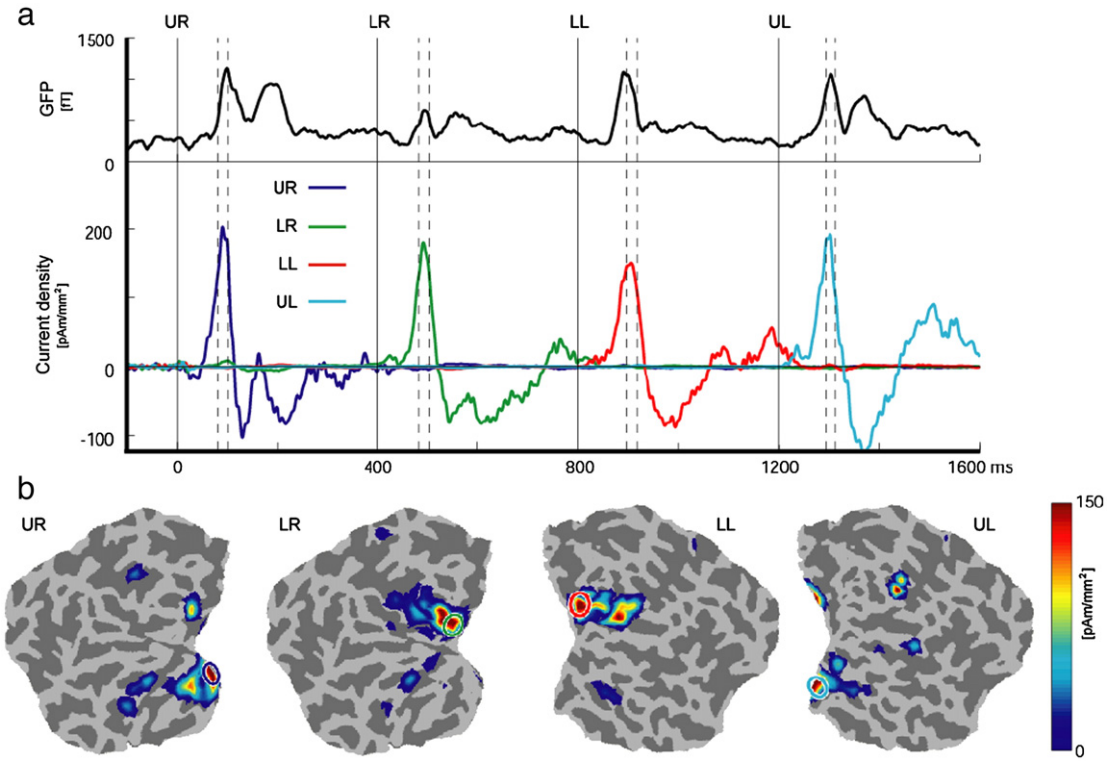

Fig. 9. Spatiotemporal pattern of the dipole currents for subject 1 in the slow RT sequence. (a) The temporal pattern of the GFP and the dipole currents in the V1 ROIs. Each color corresponds to a quadrantal visual stimulus. (b) The spatial patterns represented through TOIs whose centers are at the peaks of the dipole current time courses corresponding to the four quadrantal visual stimuli.

projected to the visual cortex in the inverse solution. To investigate this issue, we conducted hierarchical Bayesian estimation without constraint on the dipole location. That is, current dipoles were assumed on the whole cortex. The correct prior was employed with the reference hyperparameter values. Correlation coefficient with the correct prior was not significantly increased (0.81±0.11 with location constraint, 0.82±0.12 without location constraint, averaged over the 15 cases), while the temporal average of GoF within the tentative TOI (50–300 ms) was increased (78.1±4.1% with location constraint, and 87.5±3.7% without location constraint). In addition, GoF was not significantly changed at the peak of the MEG signal (96.1±1.9% with location constraint, and 96.9±1.9% without location constraint). These observations indicate that the estimated currents outside the visual cortex have no significant effect on the activity in the visual cortex.

Spatiotemporal pattern of brain activity elicited by pseudo-rotatory stimuli

The above analyses indicate that the hierarchical Bayesian method with appropriate hyperparameters provides reasonable estimation of dipole currents even when the fMRI prior is contaminated with false-positive signals. To further demonstrate the applicability of the hierarchical Bayesian method, we estimated the dipole currents for the MEG signals elicited in the RT sequence, in which the four fan-shaped stimuli were sequentially presented with an SOA much shorter than the temporal resolution of fMRI. We focused on the V1 activities, because retinotopic organization in V1 was consistently observed in estimated dipole currents for the RD sequence. The ROIs corresponding to the four visual quadrants in V1 were determined by the iterative algorithm described above.

In Fig. 9a, the upper part shows the MEG signal observed for subject 1 in the slow RT sequence. After presenting each quadrantal visual stimulus, the GFP of the MEG signal showed strong peaks with almost the same latency (92±3 ms). The lower part of Figs. 9a and b show the spatiotemporal patterns of the estimated dipole currents. The estimated V1 activities were sequentially induced in the four retinotopically organized regions of V1. The cortical locations of these ROIs were almost the same as those obtained in the RD sequence. The time courses of the dipole currents in the four V1 ROIs had almost the same shape and consisted of a first positive peak and a second negative peak, which were very similar to those observed in the RD sequence.

The upper part of Fig. 10a shows the MEG signal observed for subject 1 in the fast RT sequence. The peak latencies of the GFP were almost the same as those in the slow RT sequence (93±3 ms), although the small peaks appearing before the first and second peaks, which were observed in the slow RT sequence, disappeared. The lower part of Figs. 10a and b show the spatiotemporal pattern of the estimated dipole currents. As in the slow RT sequence, the dipole currents reproduced the retinotopic organization in V1. The latencies of the first positive peaks were almost the same (95±5 ms). Negative crosstalk currents, however, were observed just after the LR and UL stimuli.

In cases of subjects 1 and 2, the retinotopic organization in V1 was also reproduced, and similar spatiotemporal patterns

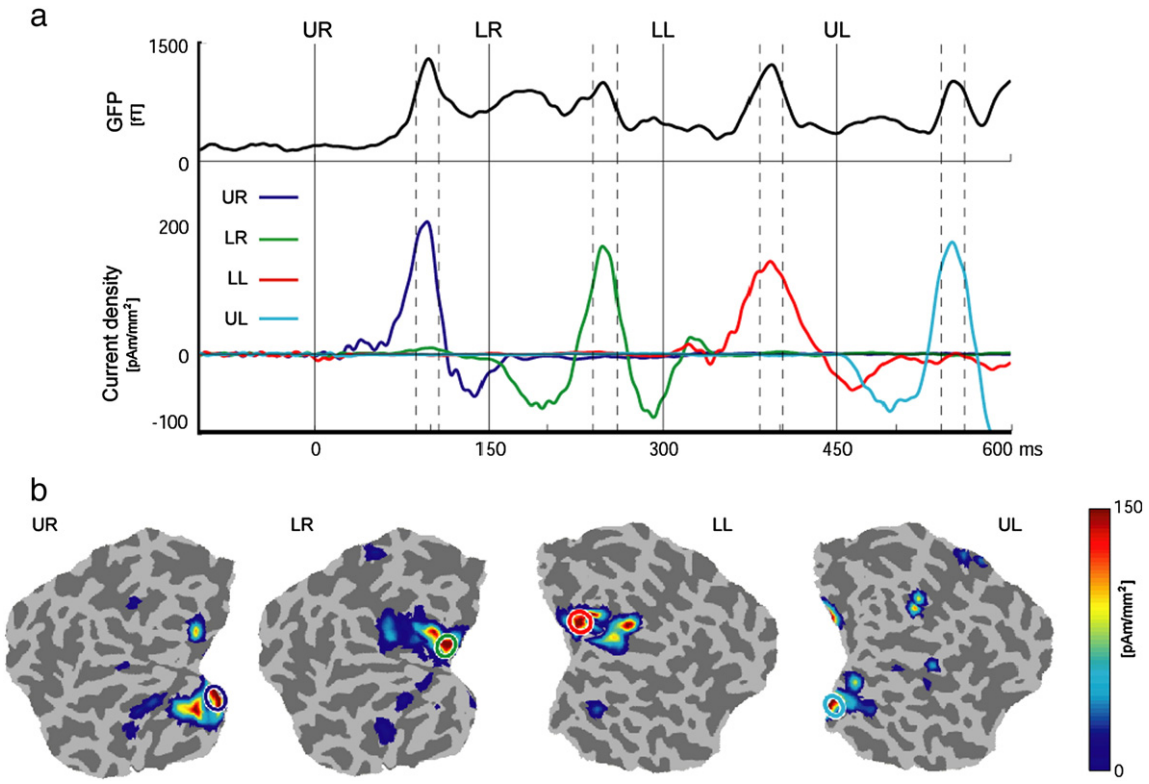

Fig. 10. Spatiotemporal pattern of the dipole currents for subject 1 in the fast RT sequence. (a) The temporal pattern of the GFP and the dipole currents in the V1 ROIs. Each color corresponds to a quadrantal visual stimulus. (b) The spatial patterns represented through TOIs whose centers are at the peaks of the dipole current time courses corresponding to the four quadrantal visual stimuli.

were observed for both the slow and fast RT sequences, although negative crosstalk was observed especially in the fast RT sequence. Since the fMRI signals of subject 4 for the UL stimulus did not show clear retinotopic organization even in V1 (see "fMRI analysis and correct/noisy priors"), we ruled this subject out from our analysis of the MEG data in the RT sequence.

The above observations indicate that the hierarchical Bayesian method enables us, with high spatial resolution, to observe fast brain activities that cannot be detected solely by fMRI.

Discussion

In this study, we evaluated the performance of the hierarchical Bayesian method for estimating neural current sources and investigated proper ranges of hyperparameters. We conducted MEG and fMRI recordings for quadrantal visual stimuli and applied the hierarchical Bayesian method to those data.

The estimation results with the reference hyperparameter values (γ_0=500, m_0=500) revealed retinotopic organization and temporal dynamics in the early visual areas, consistent with known physiological constraints. To evaluate the robustness of the hierarchical Bayesian method to false-positive activities in fMRI information, noisy priors were made from fMRI data by adding artificial false-positive activities. We confirmed that the effect of the false-positive activities in the noisy priors was effectively suppressed by employing the reference hyperparameter values. We also demonstrated that the hierarchical Bayesian method can capture the fine spatiotemporal brain activity elicited by sequential presentation of the quadrantal visual stimuli every 150 ms or 400 ms, which is much faster than the temporal resolution of fMRI.

We quantitatively evaluated the effect of hyperparameters on the spatial patterns of the estimated currents, by using the correlation coefficient and the Hamming measure. One might argue that the use of the goodness measures for the correct fMRI is a circular argument, since they use the same fMRI spatial patterns as the prior and the evaluation measure. In fact, it is a simple consequence of this fact that the correlation coefficient and the Hamming measure for the correct fMRI prior monotonically increase as the confidence parameter increases. However, we can get additional information from the goodness measures for the correct fMRI by evaluating the behavior of these measures as functions of the hyperparameters as described in "Proper range of hyperparameters". These analyses showed that the medium ranges of m_0 and γ_0 (100–1000), which include the reference value of hyperparameters, give high correlation and Hamming measures both for the correct and noisy fMRI prior and the estimated currents showed physiologically plausible results as explained above. These results cannot be obtained solely by using the correct or noisy fMRI prior.

The confidence parameter γ_0 controls the strength of the fMRI constraint on the prior current variances. According to Nummenmaa et al. (2007b), a small γ_0 (e.g., 10) gives a good result when fMRI information is not available. In this study, we showed that reliable fMRI information significantly improves spatiotemporal resolution of the estimated brain activity. In sum, the confidence parameter γ_0 can be 500, when experimental conditions of fMRI and MEG are closely matched each other as in this study. Otherwise, smaller γ_0 (e.g., 100) might be appropriate. The variance magnification parameter m_0 affected the amplitudes of the estimated currents when fMRI constraints were introduced to some extent with a medium γ_0. We showed that the estimated current amplitudes were tolerant with respect to changes in m_0. This is because the current amplitude was constrained by the MEG signal. Consequently, delicate tuning of the variance magnification parameter is not required. Fortunately, the estimated current amplitudes obtained with the reference value of m_0 roughly matched those obtained in previous electrophysiological studies. The amplitude of a neural activity depends on the type of an experimental task. The visual stimuli used in this study induce strong neural activities. In such cases, the variance magnification parameter m_0 can be as large as 500. For relatively small changes in sensory stimuli or for higher cognitive functions such as attention, the induced neural activities are expected to be small. In such cases, a certain small value of m_0 (say, 100) might be appropriate.

One might consider that the proper range of hyperparameters significantly depends on scale factors, i.e., the number of dipoles and the number of samples. When employing dipole current density as in this study, the total amplitude of dipole currents is determined from the area of the cortical surface, rather the number of dipoles. Consequently, the proper range of hyperparameters theoretically does not depend on the number of dipoles. In order to look at the effect of the number of samples, we also conducted hierarchical Bayesian estimation for a shorter duration of MEG data (50–150 ms). The profiles of goodness measures for those estimation results have similar characteristics to those shown in Figs. 5 and 6 (result not shown), indicating almost the same proper range. Although systematic evaluation and theoretical analysis are required to confirm the effect of the scale factors, we consider that the proper range of hyperparameter values is applicable for other data.

The effects of the tunable parameters of distributed source methods have been investigated with simulated data (Ahlfors and Simpson, 2004; Liu et al., 1998; Lin et al., 2006; Nummenmaa et al., 2007a; Phillips et al., 2002) and real experimental data (Nummenmaa et al., 2007b, Sharon et al., 2007). The true locations of the current sources are known in simulated data, but unknown in real data. Consequently, direct comparison of current source locations (e.g., localization error) cannot be applied for real data. In Nummenmaa et al. (2007b), the hierarchical Bayesian method was applied to visually and auditory evoked magnetic fields without using fMRI data. The authors evaluated the reconstruction error of the magnetic fields and the statistical free energy and discussed the effect of the hyperparameters when there is no fMRI data. The physiological validity of the estimated cortical activities, however, was not evaluated in detail. In this study, we investigated the physiological validity of the spatial pattern of the estimated cortical activities through comparison with the fMRI spatial pattern, under the assumption that the temporal average of the true brain activity is proportional to the fMRI signal. This assumption seems reasonable for cortical activities in the early sensory cortices, including the visual areas, although such assumptions are not always correct, especially when dealing with higher cognitive functions. The above approach for investigating validity of estimated cortical activities is similar to that employed in Sharon et al., (2007).

Current source estimation methods without anatomical information often assume dipoles on a three-dimensional grid without orientation constraints (Hashimoto et al., 2001; Moradi et al., 2003; Poghosyan and Ioannides, 2007; Sekihara et al., 2005). Since the orientations of current dipoles are estimated from MEG data, these methods are relatively insensitive to coregistration error between MEG and MRI. Although several studies have shown that localization and orientation constraints based on anatomical information improve the localization accuracy (Hillebrand and Barnes, 2003; Liu et al., 1998), coregistration error degrades the localization accuracy (Hillebrand and Barnes, 2003). Therefore, it is better to incorporate fMRI information in order to restrict the locations of cortical current sources when anatomical information is used. Therefore, in this study, we evaluated a way of incorporating fMRI information, as explained above.

Sequential activities in the early visual areas have been investigated by using multiple current dipole methods, in which the locations and orientations of the dipoles were determined with the help of fMRI information (Di Russo et al., 2005; Vanni et al., 2004). It is difficult to completely remove crosstalk in the temporal patterns of adjacent current dipoles within a few millimeters, even if the orientations of these dipoles are carefully tuned so that they are not similar (Vanni et al., 2004). In this study, we also investigated sequential activities in the early visual areas and showed that the hierarchical Bayesian method effectively suppressed crosstalk in adjacent visual areas (V1 and V2/3) in most cases, even though current dipoles were densely placed in the cortical surfaces (inter-vertex distance, 0.5–2.5 mm).

We also successfully estimated the spatiotemporal patterns of brain activities for a pseudo-rotatory visual stimulus. There are two problems, however, in dealing with such time-varying stimuli. One problem is how to incorporate fMRI priors. In this study, MEG data was temporally segmented into several time windows, and an fMRI prior corresponding to each quadrantal stimulus was assigned to each of the time windows. Such assignment is not possible when the correspondence between the stimulus and the fMRI activity is unknown. To overcome this problem, we can incorporate a number of fMRI priors and estimate their weights from MEG data (Phillips et al., 2005).

The other problem is how to determine the length of the time window. In this study, we chose 100 ms as this length. We also estimated the dipole currents by using different time windows and confirmed that there were not significant differences for these results. In general, however, there is no gold standard for the time window length. The framework for online hierarchical Bayesian estimation proposed in Sato (2001) can overcome this problem. In this framework, probabilistic variables, including the hyperparameters, are sequentially estimated at each time step by using posterior probabilities obtained in the previous time steps. Combining the above techniques expands the applicability of the hierarchical Bayesian method for noninvasive measurement of brain activity.

Acknowledgment

This research was supported in part by Japan's National Institute of Information and Communications Technology (NICT-KARC).

Appendix A. Hierarchical Bayesian model

In Sato et al. (2004), a hierarchical prior was introduced as

$$P_0(\boldsymbol{J}(\tau)|\alpha,\beta) \propto \exp\left[-\frac{\beta}{2}\boldsymbol{J}(\tau)'\boldsymbol{A}\boldsymbol{J}(\tau)\right]$$
$$P_0(\alpha) = \prod_i \mathrm{Gamma}(\alpha_i|\overline{\alpha}_{0i},\gamma_{0i}), \quad \text{(a.1)}$$
$$P_0(\beta) = 1/\beta$$
$$\mathrm{Gamma}(\alpha|\overline{\alpha},\gamma) \equiv \alpha^{-1}(\alpha\gamma/\overline{\alpha})^{\gamma}\Gamma(\gamma)^{-1}\mathrm{e}^{-\alpha\gamma/\overline{\alpha}}$$

where i is the dipole index, $\boldsymbol{A}=\mathrm{diag}(\boldsymbol{\alpha})$, $\boldsymbol{\alpha}=(\alpha_1,\ldots,\alpha_I)$, is a vector of the inverse-variance parameters for the dipole currents, β is the inverse noise variance of the observed MEG signal, and $\Gamma(\gamma)$ is the Gamma function. Each inverse-variance parameter has a Gamma distribution. $\{\boldsymbol{J}(\tau)\}_{\tau=T_{\mathrm{start}}}^{T_{\mathrm{end}}}$, α, and β are iteratively estimated by the variational Bayesian method. In the study, we use variance parameters $\nu_i \equiv \alpha_i^{-1}$, $\bar{\nu}_{0i} \equiv \bar{a}_{0i}^{-1}$, and $\rho \equiv \beta^{-1}$ since they have intuitive meaning.

Parameters of the hierarchical prior distribution, ν_{0i} and γ_{0i}, are referred to as hyperparameters. These values were determined from the fMRI information, a variance magnification parameter m_0, and a confidence parameter γ_0. γ_{0i} was set to γ_0 for all of dipoles, while ν_{0i} was set according to the fMRI t-value at each dipole and a baseline variance $\nu_{0,\mathrm{base}}$:

$$\bar{\nu}_{0i} = \nu_{0,\mathrm{base}} + (m_0 - 1)\cdot\nu_{0,\mathrm{base}}\cdot\hat{t}_i^2, \quad \text{(a.2)}$$

where $\hat{t}_i$ is a normalized fMRI-dipole t-value with a maximal value of 1. Consequently, ν_{0i} takes values from $\nu_{0,\mathrm{base}}$ to $m_0\times\nu_{0,\mathrm{base}}$. In this study, $\nu_{0,\mathrm{base}}$ was estimated from the MEG signal before the stimulus onset by using a Bayesian minimum norm method. In the Bayesian minimum norm estimation of $\nu_{0,\mathrm{base}}$, all dipoles were assumed to have the same prior current variance $\rho_{\mathrm{base}}\times\nu_{0,\mathrm{base}}$, where ρ_{base} is the noise variance before the stimulus onset. Although ρ_{base} was also estimated simultaneously with $\nu_{0,\mathrm{base}}$, this value was not used for setting the hyperparameters.

According to the first equation of (Eq. (a.1)), the prior current variance is $\rho\times\nu_i$. Namely, the noise variance ρ is also a scaling factor for the prior current variance.

Appendix B. Smoothness constraint on cortical current distribution

Under the quasistatic approximation assumption (Hamalainen et al., 1993), the MEG forward model, i.e., the relationship between the amplitudes of the current dipoles and the observed magnetic field at time point τ, is given by

$$\boldsymbol{B}(\tau) = \boldsymbol{G}\cdot\boldsymbol{J}(\tau), \quad \text{(a.3)}$$

where $\boldsymbol{B}(\tau)$ is an N-element vector for the magnetic field, $\boldsymbol{J}(\tau)$ is an I-element vector for the current amplitudes, and $\boldsymbol{G}$ is an N-by-I matrix, referred to as the lead field.

In this study, we assumed a spatial smoothness constraint on the current distribution. To do this, we employed a smoothing matrix $\boldsymbol{W}_{ij} \propto \exp(-d_{ij}^2/R^2)$, where d_{ij} is the distance between the i-th and j-th current dipoles along the cortical surface, and the smoothing radius parameter R was set to give a FWHM of 8 mm. By introducing an auxiliary variable $\boldsymbol{Z}(\tau)$ and letting

$$\boldsymbol{J}(\tau) = \boldsymbol{W}\cdot\boldsymbol{Z}(\tau), \quad \text{(a.4)}$$

Eq. (a.4) can be replaced by

$$\boldsymbol{B}(\tau) = \hat{\boldsymbol{G}} \cdot \boldsymbol{Z}(\tau), \tag{a.5}$$

where $\hat{\boldsymbol{G}} \equiv \boldsymbol{G} \times \boldsymbol{W}$ is a smoothed lead field matrix. Therefore, the inverse problem becomes the problem of estimating $\boldsymbol{Z}(\tau)$ with the smoothed lead field matrix $\hat{\boldsymbol{G}}$. After estimating $\boldsymbol{Z}(\tau)$, the actual current $\boldsymbol{J}(\tau)$ is obtained from Eq. (a.4).

References

Aine, C., Huang, M., Stephen, J., Christner, R., 2000. Multistart algorithms for MEG empirical data analysis reliably characterize locations and time courses of multiple sources. Neuroimage 12, 159–172.

Ahlfors, S.P., Simpson, G.V., 2004. Geometrical interpretation of fMRI-guided MEG/EEG inverse estimates. Neuroimage 22 (1), 323–332.

Ahlfors, S.P., Simpson, G.V., Dale, A.M., Belliveau, J.W., Liu, A.K., Korvenoja, A., Virtanen, J., Huotilainen, M., Tootell, R.B.H., Aronen, H.J., Ilmoniemi, R.J., 1999. Spatiotemporal activity of a cortical network for processing visual motion revealed by MEG and fMRI. J. Neurophesiol. 82 (5), 2545–2555.

Bandettini, P.A., 2000. The temporal resolution of functional MRI. In: Moonen, C.T.W., Bandettini, P.A. (Eds.), Functional MRI. Springer, Berlin, pp. 205–220.

Belliveau, J.W., Kennedy, D.N., McKinstry, R.C., Buchbinder, B.R., Weisskoff, R.M., Cohen, M.S., Vevea, J.M., Brady, T.J., Rosen, B.R., 1991. Functional mapping of the human visual cortex by magnetic resonance imaging. Science 254, 716–719.

Brewer, A.A., Liu, J., Wade, A.R., Wandell, B.A., 2005. Visual field maps and stimulus selectivity in human ventral occipital cortex. Nat. Neurosci. 8 (8), 1102–1109.

Dale, A.M., Sereno, M.I., 1993. Improved localization of cortical activity by combining EEG and MEG with MRI cortical surface reconstruction: a linear approach. J. Cogn. Neurosci. 5, 162–176.

Dale, A.M., Fischl, B., Sereno, M.I., 1999. Cortical surface-based analysis. I: Segmentation and surface reconstruction. Neuroimage 9, 179–194.

Dale, A.M., Liu, A.K., Fischl, B.R., Buckner, R.L., Belliveau, J.W., Lewine, J.D., Halgren, E., 2000. Dynamic statistical parametric mapping: combining fMRI and MEG for high-resolution imaging of cortical activity. Neuron 26 (1), 55–67.

Di Russo, F., Martinez, A., Sereno, M.I., Pitzalis, S., Hillyard, S.A., 2001. Cortical sources of the early components of the visual evoked potential. Hum. Brain Mapp. 15 (2), 95–111.

Di Russo, F., Pitzalis, S., Spitoni, G., Aprile, T., Patria, F., Spinelli, D., Hillyard, S.A., 2005. Identification of the neural sources of the pattern-reversal VEP. Neuroimage 24, 874–886.

Dougherty, R.F., Koch, V.M., Brewer, A.A., Fischer, B., Modersitzki, J., Wandell, B.A., 2003. Visual field representations and locations of visual areas V1/2/3 in human visual cortex. J. Vision 3, 586–598.

Hamalainen, M.S., Ilmoniemi, R.J., 1994. Interpreting magnetic fields of the brain: minimum norm estimates. Med. Biol. Eng. Comput. 32, 35–42.

Hamalainen, M.S., Hari, R., Ilmoniemi, R.J., Knuutila, J., Lounasmaa, O.V., 1993. Magnetoencephalography — theory, instrumentation, and applications to non-invasive studies of the working human brain. Rev. Modern Phys. 65, 413–497.

Hari, R., 1991. On brain's magnetic responses to sensory stimuli. J. Clin. Neurophysiol. 8, 157–169.

Hashimoto, I., Kimura, T., Iguchi, Y., Takino, R., Sekihara, K., 2001. Dynamic activation of distinct cytoarchitectonic areas of the human SI cortex after median nerve stimulation. Neuroreport 12 (9), 1891–1897.

Hillebrand, A., Barnes, G.R., 2003. The use of anatomical constraints with MEG beamformers. Neuroimage 20 (4), 2302–2313.

Jerbi, K., Baillet, S., Mosher, J.C., Nolte, G., Garnero, L., Leahy, R.M., 2004. Localization of realistic cortical activity in MEG using current multipoles. Neuroimage 22 (2), 779–793.

Kajihara, S., Ohtani, Y., Goda, N., Tanigawa, M., Ejima, Y., Toyama, K., 2004. Wiener filter-magnetoencephalography of visual cortical activity. Brain Topogr. 17, 13–25.

Lin, F.H., Belliveau, J.W., Dale, A.M., Hamalainen, M.S., 2006. Distributed current estimates using cortical orientation constraints. Hum. Brain Mapp. 27, 1–13.

Liu, A.K., Belliveau, J.W., Dale, A.M., 1998. Spatiotemporal imaging of human brain activity using functional MRI constrained magnetoencephalography data: Monte Carlo simulations. Proc. Natl. Acad. Sci. 95, 8945–8950.

Logothetis, N.K., Pauls, J., Augath, M., Trinath, T., Oeltermann, A., 2001. Neurophysiological investigation of the basis of the fMRI signal. Nature 412, 128–130.

Miltner, W., Braun, C., Johnson, R., Simpson, G.V., Ruchkin, D.S., 1994. A test of brain electrical source analysis (BESA): a simulation study. Electroencephalogr. Clin. Neurophysiol. 91 (4), 295–310.

Moradi, F., Liu, L.C., Cheng, K., Waggoner, R.A., Tanaka, K., Ioannides, A.A., 2003. Consistent and precise localization of brain activity in human primary visual cortex by MEG and fMRI. Neuroimage 18 (3), 595–609.

Mosher, J.C., Leahy, R.M., Lewis, P.S., 1999. EEG and MEG: forward solutions for inverse methods. IEEE Trans. Biomed. Eng. 46, 245–259.

Mosher, J.C., Lewis, P.S., Leahy, R.M., 1992. Multiple dipole modeling and localization from spatio-temporal MEG data. IEEE Trans. Biomed. Eng. 39, 541–557.

Nummenmaa, A., Auranen, T., Hamalainen, M.S., Jaaskelainen, I.P., Sams, M., Vehtari, A., Lampinen, J., 2007a. Hierarchical Bayesian estimates of distributed MEG sources: theoretical aspects and comparison of variational and MCMC methods. Neuroimage 35 (2), 669–685.

Nummenmaa, A., Auranen, T., Hamalainen, M.S., Jaaskelainen, I.P., Sams, M., Vehtari, A., Lampinen, J., 2007b. Automatic relevance determination based hierarchical Bayesian MEG inversion in practice. Neuroimage 37 (2), 876–889.

Nunez, P.L., 1981. Electric Fields of the Brain: The Neurophysics of EEG. Oxford Univ. Press, New York.

Ogawa, S., Lee, T.M., Kay, A.R., Tank, D.W., 1990. Brain magnetic resonance imaging with contrast dependent oxygenation. Proc. Natl. Acad. Sci. U. S. A. 87, 9868–9872.

Pascual-Marqui, R.D., 1999. Review of methods for solving the EEG inverse problem. Int. J. Bioelectromagn. 1, 75–86.

Pascual-Marqui, R.D., Michel, C.M., Lehmann, D., 1994. Low resolution electromagnetic tomography: a new method for localizing electrical activity in the brain. Int. J. Psychophysiol. 18, 49–65.

Phillips, C., Rugg, M.S., Friston, K.J., 2002. Anatomically informed basis functions for EEG source localization: combining functional and anatomical constraints. Neuroimage 16, 678–695.

Phillips, C., Mattout, J., Rugg, M.D., Maquet, P., Friston, K.J., 2005. An empirical Bayesian solution to the source reconstruction problem in EEG. Neuroimage 24 (4), 997–1011.

Poghosyan, V., Ioannides, A.A., 2007. Precise mapping of early visual responses in space and time. Neuroimage 35 (2), 759–770.

Sato, M., 2001. On-line model selection based on the variational Bayes. Neural Comput. 13, 1649–1681.

Sato, M., Yoshioka, T., Kajihara, S., Toyama, K., Goda, N., Doya, K., Kawato, M., 2004. Hierarchical Bayesian estimation for MEG inverse problem. Neuroimage 23, 806–826.

Scherg, M., Bast, T., Berg, P., 1999. Multiple source analysis of interictal spikes: goals, requirements, and clinical value. J. Clin. Neurophysiol. 16 (3), 214–224.

Schmidt, D.M., George, J.S., Wood, C.C., 1999. Bayesian inference applied to the electromagnetic inverse problem. Hum. Brain Mapp. 7, 195–212.

Sekihara, K., Sahani, M., Nagarajan, S.S., 2005. Localization bias and spatial resolution of adaptive and non-adaptive spatial filters for MEG source reconstruction. Neuroimage 25 (4), 1056–1067.

Sereno, M.I., Dale, A.M., Reppas, J.B., Kwong, K.K., Belliveau, J.W., Brady, T.J., Rosen, B.R., Tootell, R.B.H., 1995. Borders of multiple visual areas in humans revealed by functional magnetic resonance imaging. Science 268, 889–893.

Sharon, D., Hamalainen, M.S., Tootell, R.B.H., Halgren, E., Belliveau, J.W., 2007. The advantage of combining MEG and EEG: comparison to fMRI in focally stimulated visual cortex. Neuroimage 36 (4), 1225–1235.

Tissari, S., Rahola, J., 2003. Error analysis of a Galerkin method to solve the forward problem in MEG using the boundary element method. Comput. Methods Programs Biomed. 72 (3), 209–222.

Tootell, R.B.H., Dale, A.M., Sereno, M.I., Malach, R., 1997. New images from human visual cortex. Trends Neurosci. 19 (11), 481–489.

Uutela, K., Hamalainen, M.S., Somersalo, E., 1999. Visualization of magnetoencephalographic data using minimum current estimates. Neuroimage 10, 173–180.

Vanni, S., Tansakanen, T., Seppa, M., Uutela, K., Hari, R., 2001. Coinciding early activation of the human primary visual cortex and anteromedial cuneus. Proc. Natl. Acad. Sci. 98 (5), 2776–2780.

Vanni, S., Warnking, J., Dojat, M., Delon-Martin, C., Bullier, J., Segebarth, C., 2004. Sequence of pattern onset responses in the human visual areas: an fMRI constrained VEP source analysis. Neuroimage 21 (3), 801–817.

Wang, J.Z., Williamson, S.J., Kaufman, L., 1992. Magnetic source images determined by a lead-field analysis: the unique minimum-norm least-squares estimation. IEEE Trans. Biomed. Eng. 39, 665–675.